Faculty of Science

Streamlined landform distribution in south-west Sweden

Andreas V. Lundell

Degree of Bachelor of Science
with a major in Earth Sciences
15 hec

Department of Earth Sciences
University of Gothenburg
2020 B-1098

UNIVERSITY OF GOTHENBURG

UNIVERSITY OF GOTHENBURG
Department of Earth Sciences
Geovetarcentrum/Earth Science Centre

Streamlined landform distribution in south-west Sweden

Andreas V. Lundell

ISSN 1400-3821

B1098
Bachelor of Science thesis
Göteborg 2020

Mailing address
Geovetarcentrum
S 405 30 Göteborg

Address
Geovetarcentrum
Guldhedsgatan 5A

Telephone
031-786 19 56

Geovetarcentrum
Göteborg University
S-405 30 Göteborg
SWEDEN

Abstract

Streamlined landforms are forming underneath today's glaciers. Since the Earth is undergoing a deglaciation it is important to understand how the glaciers move over the landscape to be able to predict future changes. In order to better understand the current deglaciation we can look to the past one and to that end a 14 085 km² area of south-western Sweden was mapped. Using a high resolution hillshaded DTM derived from a DEM created using LiDAR data (spatial resolution of 2 m) a map of the distribution and the ice flow direction of streamlined glacial landforms, with a focus on stoss-side moraines and crag-and-tails was created.

It was found that the dominant ice flow direction was towards the south-west in south-western Sweden. Furthermore, stoss-side moraines were more common towards the coastline where the land is well below the highest coastline, whereas the number of crag-and-tails were few. Only the two most narrow bedrock knobs of the stoss-side moraines were smaller than the biggest bedrock knob of the crag-and-tails and on average the stoss-side moraines bedrock knob was 10,3 times wider than that of the crag-and-tails. The stoss-side moraines and crag-and-tails are both formed around a bedrock knob. The stoss-side moraines have sediment on the proximal (i.e. up-ice) side, whereas the crag-and-tails have sediment on the distal (i.e. down-ice) side of the bedrock knob.

Streamlined till patches often contained multiple streamlined features which had merged into one suggesting that they are deposited wherever their formation is promoted. Another key finding was that there is always a taller mountain peak up-ice from every stoss-side moraine and often also a low laying flat directly up-ice from the stoss-side moraine, both of which appear to be crucial to their formation. Furthermore, two primary flow directions were indicated by the crag-and-tails, the first towards approximately 210° and the second towards approximately 240°. This is explained by their position on the land with all of the crag-and-tails with an azimuth of 220° or less being on the eastern side. An alternative explanation is that the crag-and-tails trending towards 240° are older, forming during the initial advance and those trending towards 210° being deposited during a readvance or during a retreat.

Table of Contents

1. Introduction

Glaciers deposit a multitude of different landforms, some of which are streamlined, which means they align themselves with the ice flow direction during formation (Benn & Evans, 2014, p. 260). In general, streamlined landforms can produce an eminence that is shaped by a glacier moving over a hard obstacle, like bedrock or a boulder, along with the erosion of the softer surrounding material. Typically, sediment also flows into the cavity that forms. Streamlined landforms include but are not limited to: stoss-side moraines, crag-and-tails, drumlins, flutes, whalebacks (Benn & Evans, 2014, pp. 260-282).

These landforms are currently being deposited underneath the present-day glaciers (Smith et al., 2007; Johnson et al., 2010) and during the Earth's current deglaciation the glacier's movements are unpredictable (Stearns & Hamilton, 2007; Howat et al., 2011). To better understand how the glaciers will behave during this deglaciation we can look to the past. According to the law of uniformitarianism (Marshak, 2015, p. 437), it is possible to study the past deglaciation that took place after the last glacial maximum (LGM) and the glacial landforms associated with it in order to understand the current one. A deep understanding of the subglacial landforms can help predict immediate future changes to today's glaciers.

This study investigates the following question: What is the distribution of streamlined landforms in south-west Sweden and why do they occur where they occur?

This study focuses on two subglacial streamlined landforms: stoss-side moraine (referred to as precrag ridge by Gillberg (1976) and Haavisto-Hyvärinen (1996) and stoss-side moraine by Hillefors (1973)) and crag-and-tails. Stoss-side moraines and crag-and-tails are similar in that they often appear together and have a bedrock knob protecting the sediment, though the former forms on the stoss (up-ice) side and the latter forms on the lee (down-ice) side.

According to Hillefors (1973), stoss-side moraines are formed by abrasion and frost weathering of the bedrock up-ice and subsequent deposition of sediment down-ice, though an endogenous origin (i.e. sediment originating from where it's deposited) is also plausible. Thus, stoss-side moraines are large ridges that have a grounding bedrock knob on the lee side (Hillefors, 1973). They have most likely been built up over more than one past glaciation since sediment that is older than the last glaciation has been found in the four stoss-side moraines that have been excavated. (Hillefors, 1973; Påsse, 1998).

Crag-and-tails form as the ice moves over a raised resistant bedrock knob, creating a cavity down-ice where the surrounding weaker rock and sediment material can accumulate and is thus protected from further erosion by the hard bedrock knob (Benn & Evans, 2014, p. 281). This means that crag-and-tails are elongated ridges mostly made of till that form on the lee side with a bedrock knob on the stoss-side.

Additionally, there are streamlined till patches that are neither stoss-side moraines nor crag-and-tail ridges. They could be stoss-side moraines or crag-and-tails where the bedrock knob has been covered by sediment. Some of these till patches have poorly defined crag-and-tails in

them, others form a collection of stoss-side moraines and crag-and-tails which have all merged into one large feature. However, the most important detail is that they all have streamlined qualities to them. Though these do not indicate ice flow direction, their axes are generally similar to those shown by the mapped stoss-side moraines and crag-and-tails.

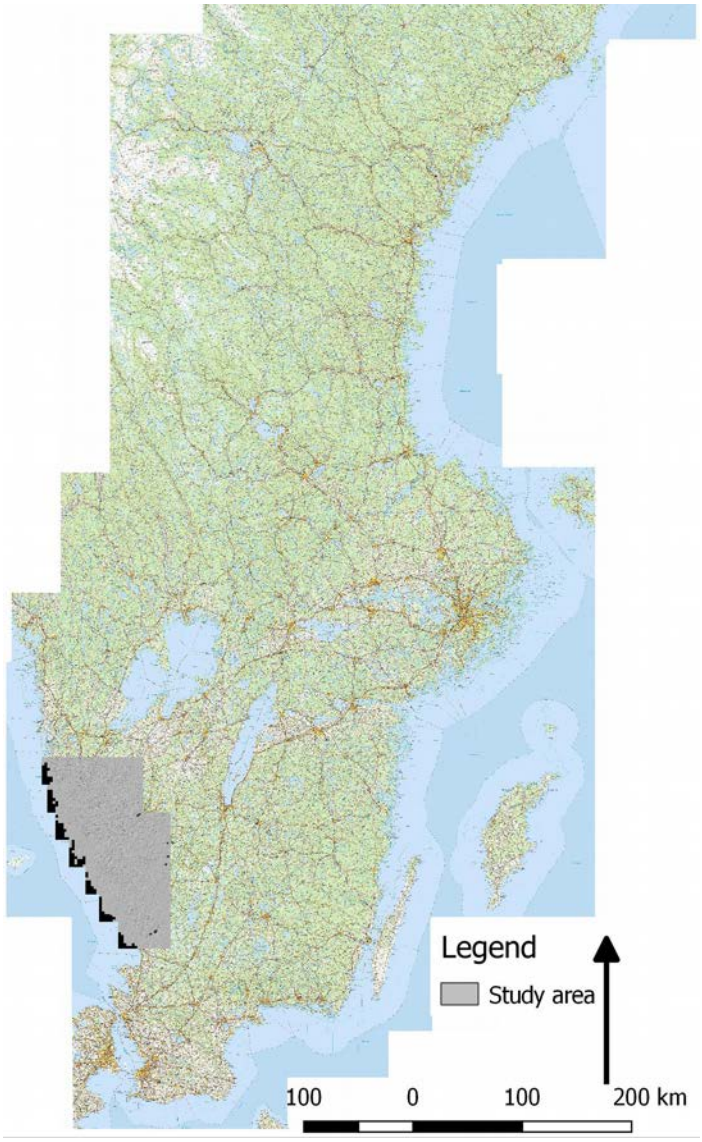

Figure 1. An overview map of the study area in grey scaled LiDAR images.

The study area in Figure 1 covers a region of 14 085 km² and is located in the south-west of Sweden. This study area was chosen because many streamlined landforms can be found in the region (Gillberg, 1976; Hillefors, 1973). This region is characterised by its joint valley landscape with some eskers and endmoraines and streamlined landforms can be found (Engdahl & Påsse, 2014). The bedrock is mainly hard granitic bedrock which to varying degrees is covered by till with a lot of clay and silt lain on top of it (SGU, 2020) following the isostatic uplift since much of south-western Sweden was below the highest coastline. (Dowling, Spagnolo & Möller, 2015; Engdahl & Påsse, 2014).

Previous studies used Light detection and ranging (LiDAR) in order to identify streamlined landforms in southern Sweden (Dowling et al., 2015; Bouvier, Johnson & Påsse, 2015). However, these studies covered other parts of southern Sweden. Further, the study by Dowling et al. (2015) focused on the morphometry of the landforms rather than the distribution.

2. Method

2.1 LiDAR data used

LiDAR images in the form of a digital elevation model (DEM) were sourced from Lantmäteriet. The LiDAR images were pre-processed to where all the laser data points that were not on ground level were removed, leaving a detailed image of the landform surface. From this DEM a terrain model using hillshade (azimuth of the light at 315°, altitude at 45°, Z factor and scale at 1) was produced in order to better visualise the features. An azimuth of 315° was chosen because it made the features in the study area stand out the most.

The DEM and terrain model, both with a spatial resolution of 2 meters (Lantmäteriet, 2020), were then added into the selected geographic information systems (GIS) program QGIS[1] (version 2.18.4). Using these tools, glacial landforms, specifically stoss-side moraines, streamlined till patches and crag-and-tails were mapped and analysed.

2.2 The mapped features

All of the streamlined till patches show indications of streamlining on them, however, not all of them outline a stoss-side moraine (see Figures 2-3). All streamlined till patches were mapped by outlining their entire extent with a polygon and for the streamlined till patches that were stoss-side moraines a line was also added on top to indicate the ice flow direction, whereas the length and ice flow direction were mapped for the crag-and-tails. Furthermore, the width of all bedrock knobs for the stoss-side moraines and crag-and-tails were recorded in order to determine if there is a threshold at which one landform is preferentially deposited. When necessary, a Geological Survey of Sweden (SGU) soil map was used to aid in determining features, with all types of till in one colour and rock in another.

The reason for mapping using LiDAR images is to view the ground as it would look like without vegetation or anthropogenic structures (see Figure 3). This makes it possible to make out the outlines of landforms as seen from above. The choice of QGIS was motivated by two primary reasons, the first is the authors familiarity with the program, the second is the program's availability, with it being open source software (Steiniger, 2009).

All features were then put into a table in order to compare the different features between and against each other to see if there is some commonality in the mapped parameters. With this data two rose diagrams were made to make it easier to visualise the ice flow direction. For this purpose the program GeoRose[2] was used. The choice of GeoRose was motivated by its availability as well as its ease of use.

1 https://www.qgis.org/en/site/
2 http://www.yongtechnology.com/download/georose

2.3 How features were selected

When mapping there was a focus on clearly defined and distinct features and thus, they are over represented in the data. More streamlined features can be observed in the study area. The criteria for adding a stoss-side moraine was for the width of the ridge to not exceed the width of the bedrock knob. The ridge also had to be limited by a bedrock knob on the down-ice side. It was also important to have at least one side of the ridge to be distinct. The criteria for adding a crag-and-tail was for it to be possible to tell where the bedrock knob started and the till tail ended. Here it was crucial to be able to make out the outline and extent of the tail ridge using the map alone. The crag also had to be wider than the tail. For a feature to be mapped as a streamlined till patch it had to show clear indications of streamlining, but the entire till patch could not align itself with the ice flow direction. Bedrock knobs were excluded to the extent that it was possible and their outline had to be visible on the map.

Figures 2-3 show how the mapping was done. Also included in Figure 2 is an SGU soil map which was sometimes used in order to make it easier when determining features. The red areas are all types of hard rock and the pale yellow areas are all types of till. In Figure 3, the red arrows point to the bedrock knobs of the stoss-side moraines, the pink arrows point to crag-and-tails and the blue arrows point to streamlined till patches (4 of which are also associated with a stoss-side moraine)

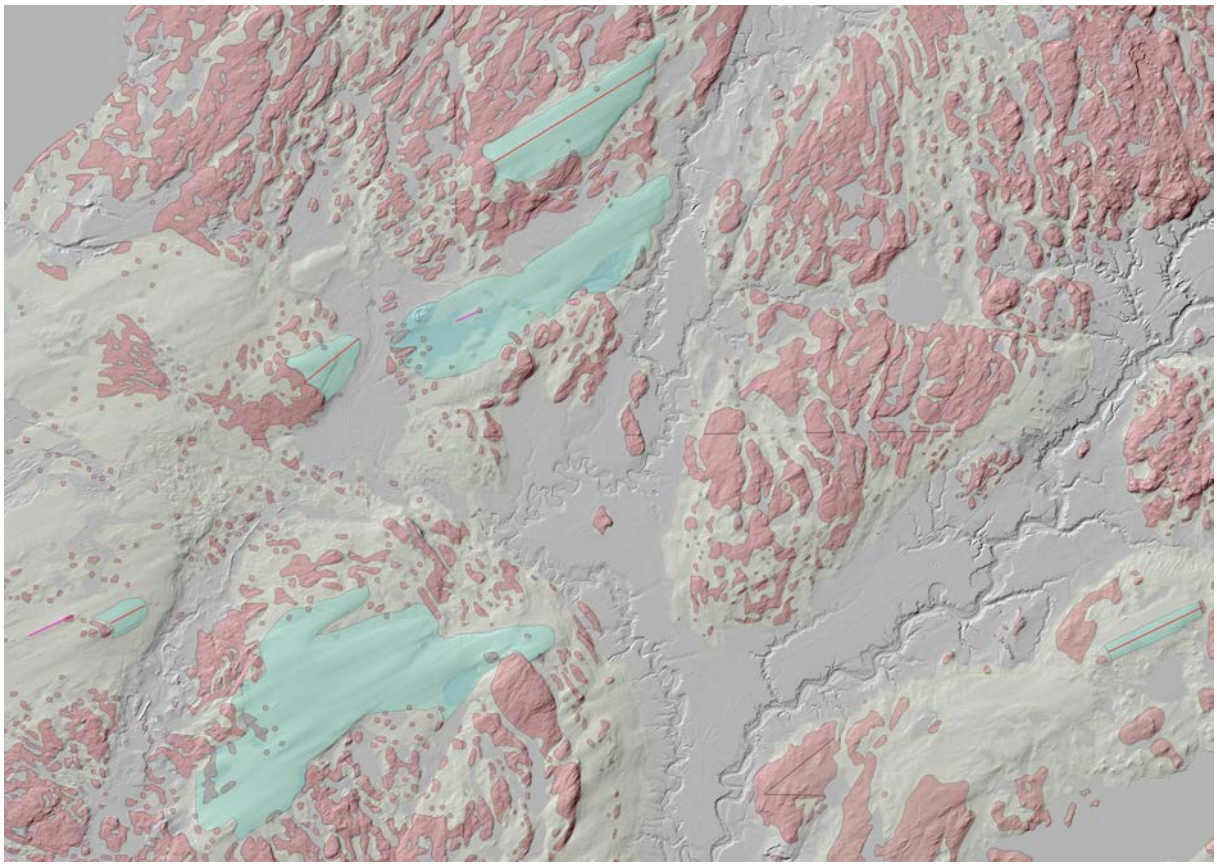

Figure 2. Map showing how the features were mapped. The blue areas are streamlined till patches, the red lines are stoss-side moraines and the pink lines are crag-and-tails.

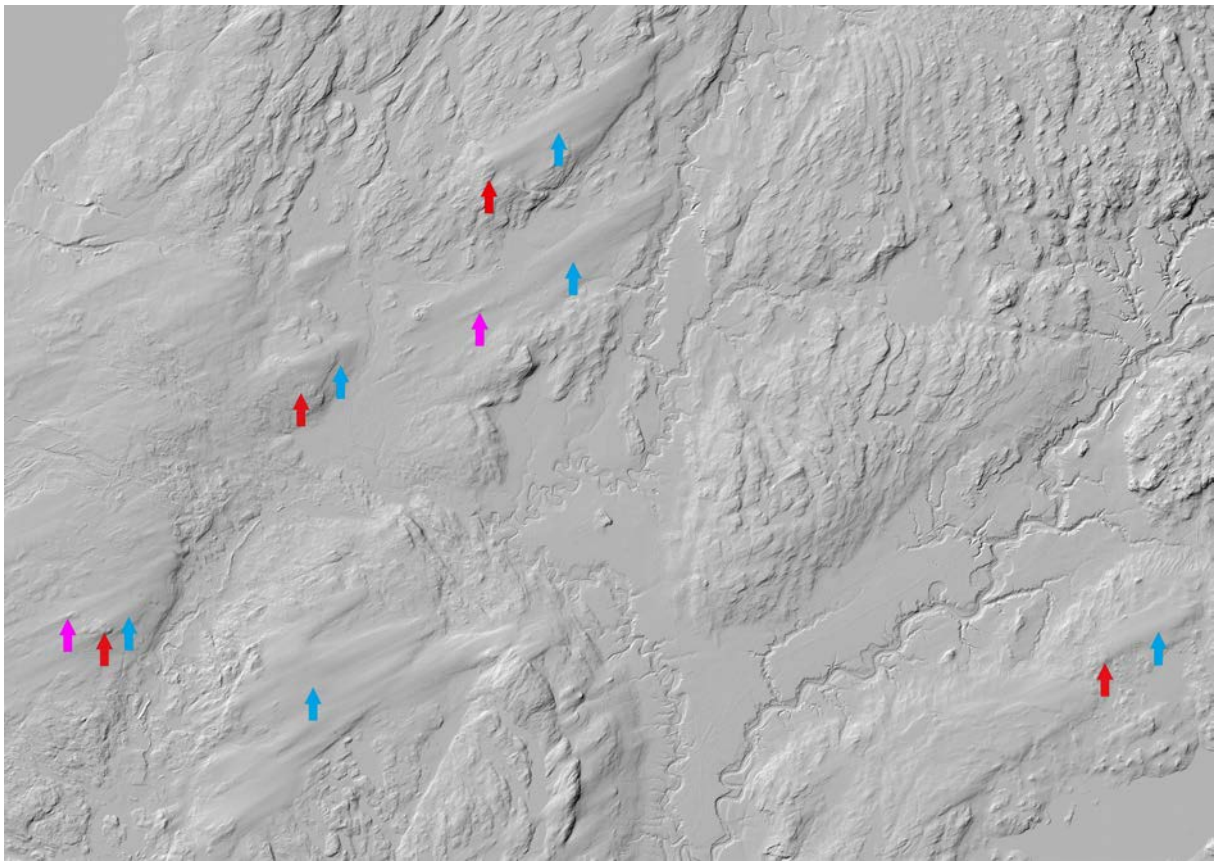

Figure 3. Map showing the hillshaded terrain model shown in Figure 2 without any mapped features.

3. Results

An overview map is presented in Figure 4 and maps of the sections are presented in Figures 5-7, with the extent of these outlined in Table 1. For more detailed renderings see Appendix B.

Section	North-west coordinates	South-east coordinates
Northern	N58,137695° E11,305046°	N57,724728° E12,901149°
Middle	N57,695376° E11,560113°	N57,057552° E13,351213°
Southern	N57,038878° E12,280603°	N56,608549° E13,370831°

Table 1. Geographical extent of the different sections in Figures 5-7. Listed in the WGS84 CRS.

The northern section (Figure 5), is characterised by exposed bedrock and relatively little till cover. Despite this there is a total of 14 stoss-side moraines and 6 crag-and-tails along with 2 streamlined till patches in the section. Further, the middle section (Figure 6) contains the most features with 49 stoss-side moraines, 45 crag-and-tails along with 24 streamlined till patches. Finally, the southern section (Figure 7) is at the lowest elevation above sea level and thus more features in this region are covered by sediment. There is a total of 10 stoss-side moraines, 9 crag-and-tails and 3 streamlined till patches. A total of 93 streamlined till patches can be found in the study area, of which 73 are stoss-side moraines. There are also 60 crag-and-tails.

3.1 The map of the study area

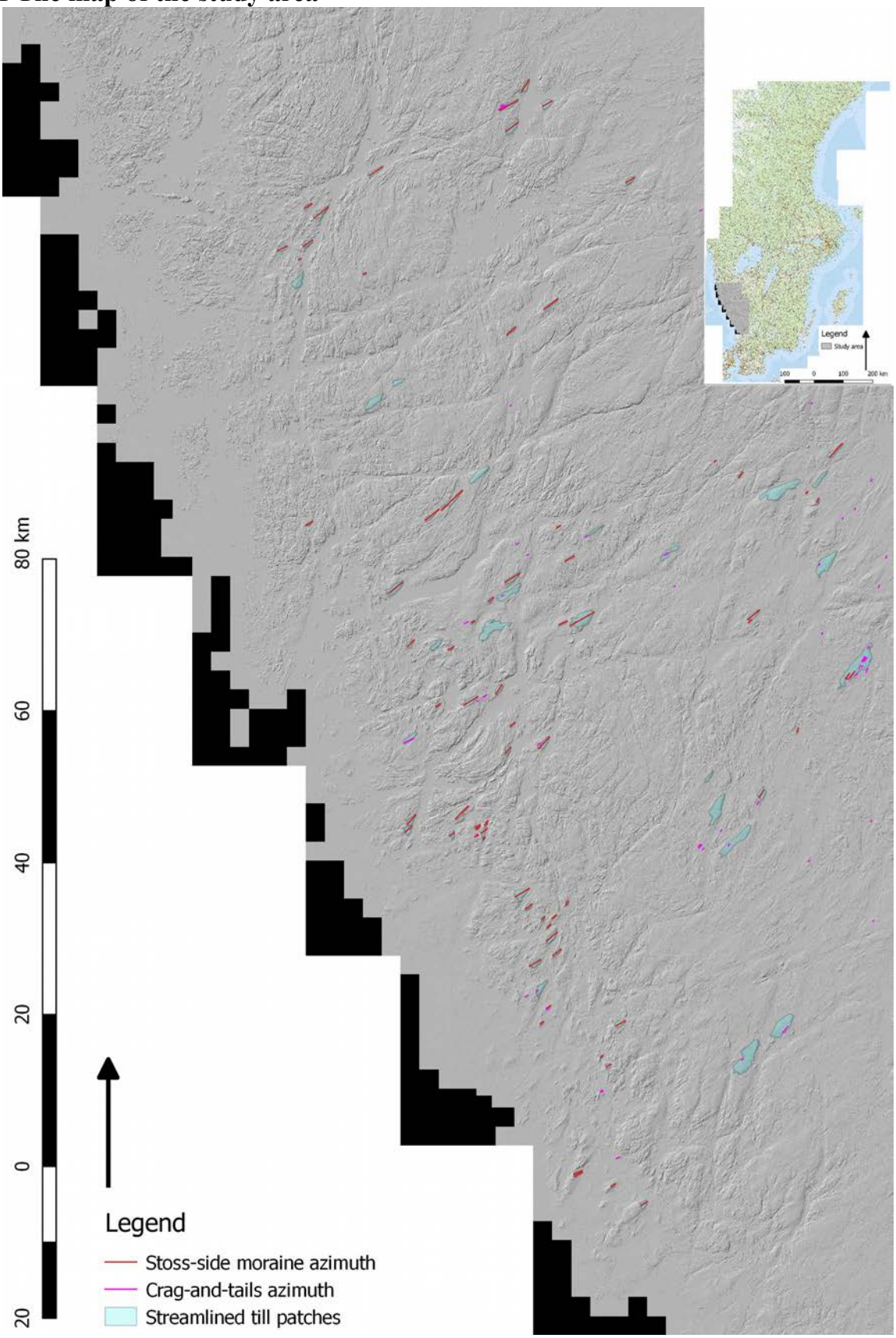

Figure 4. The map of the whole area, showing the distribution of the features.

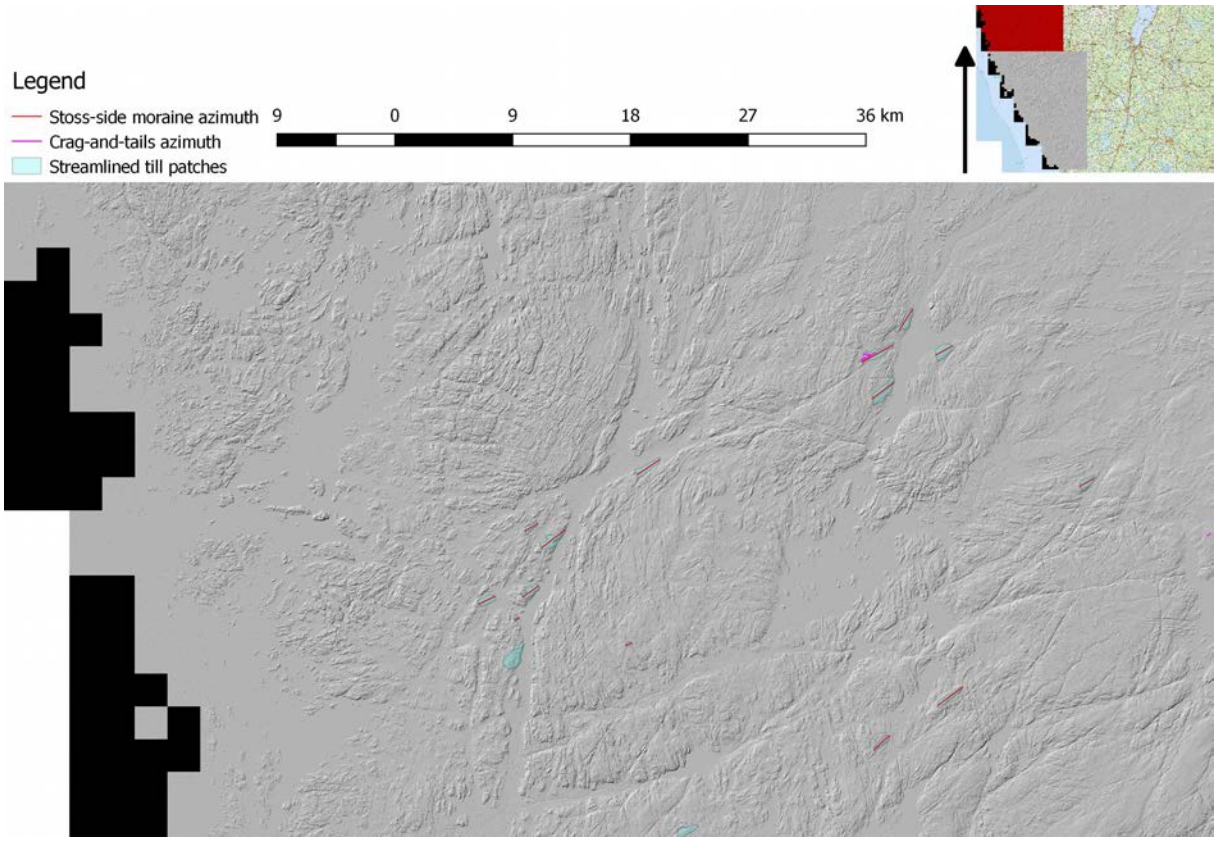

Figure 5. Northern section. This section is characterised by exposed bedrock and fairly little till cover.

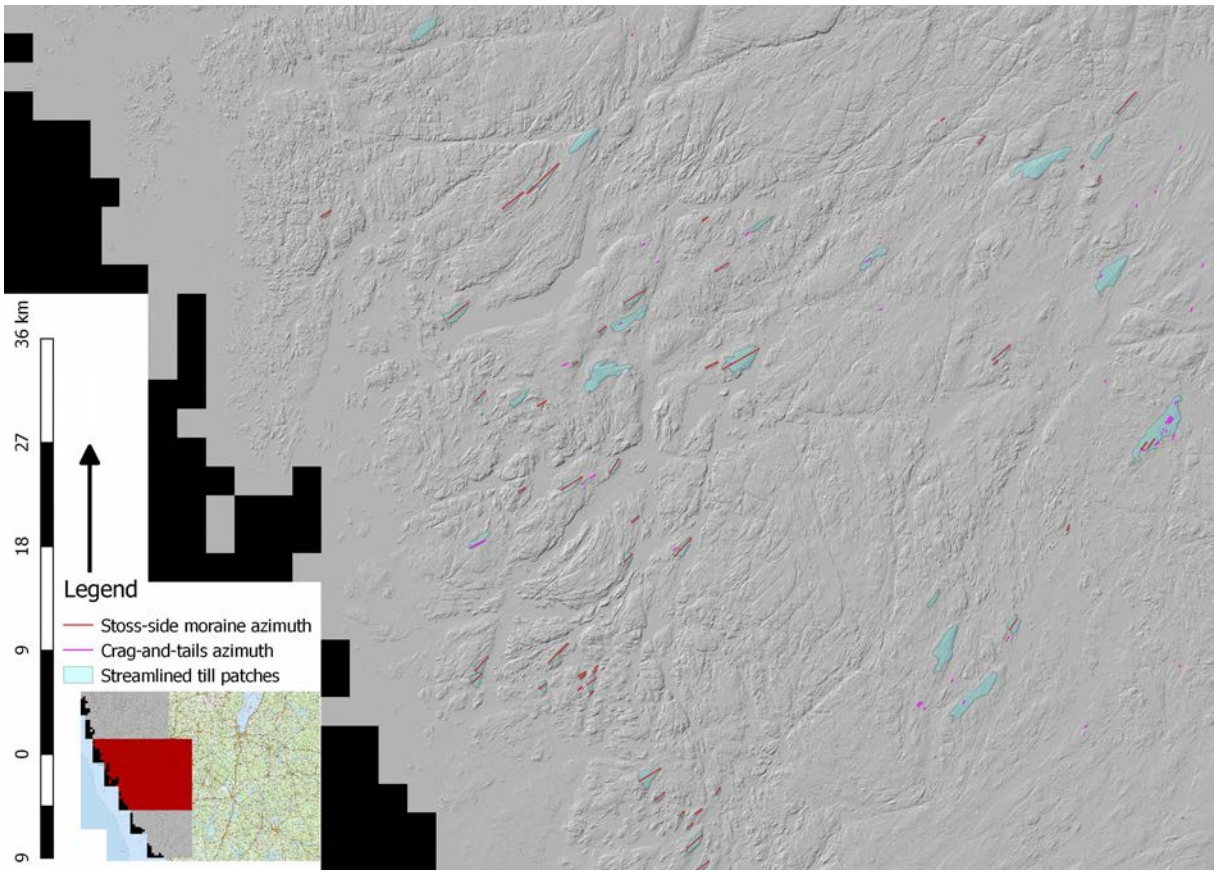

Figure 6. Middle section. This section contains the most features.

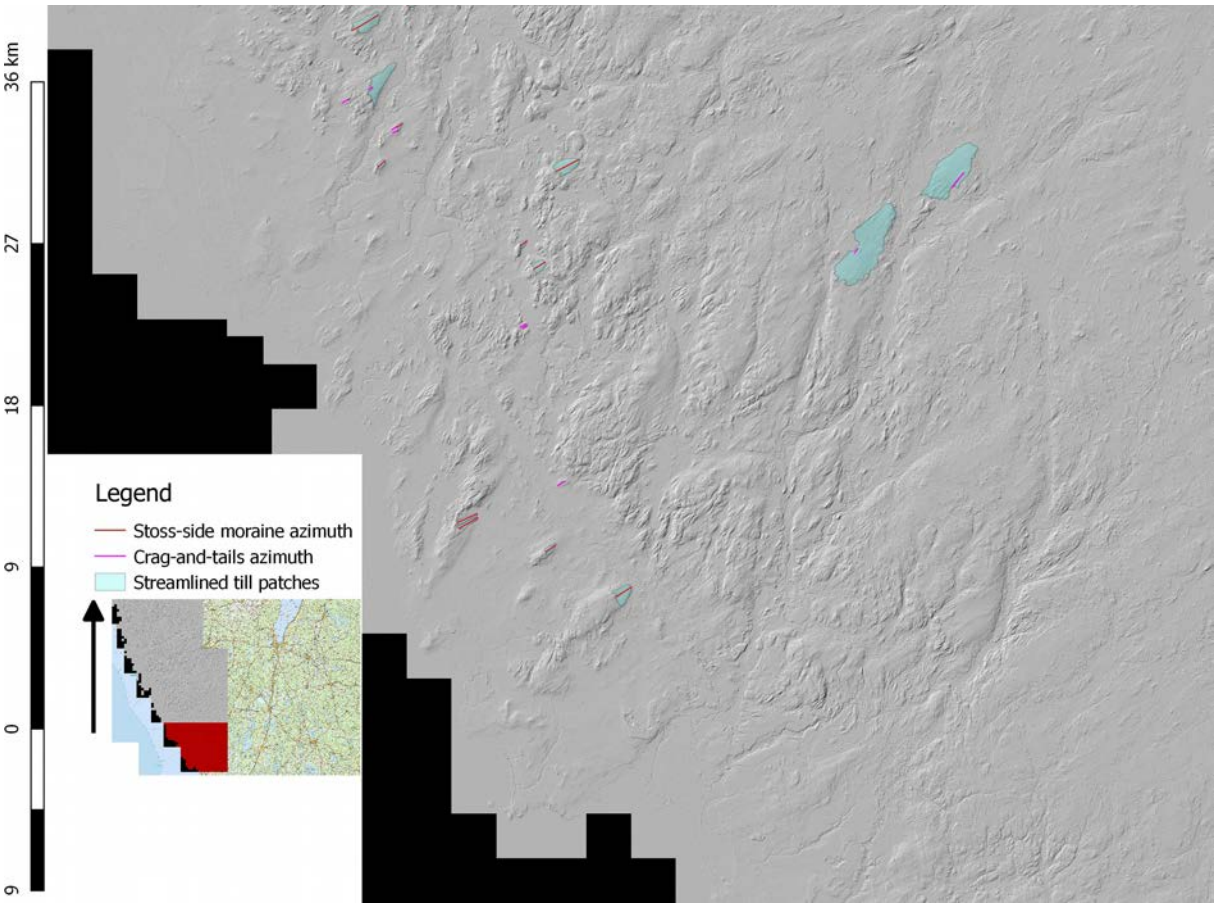

Figure 7. Southern section. This section is at the lowest elevation above sea level and thus more features in this region are covered by sediment.

3.2 Rose diagram of features

Figures 8-9 present two rose diagrams that show the azimuth (i.e. ice flow direction) of all crag-and-tails and all stoss-side moraines respectively. Both diagrams used a diagram interval of 3 degrees.

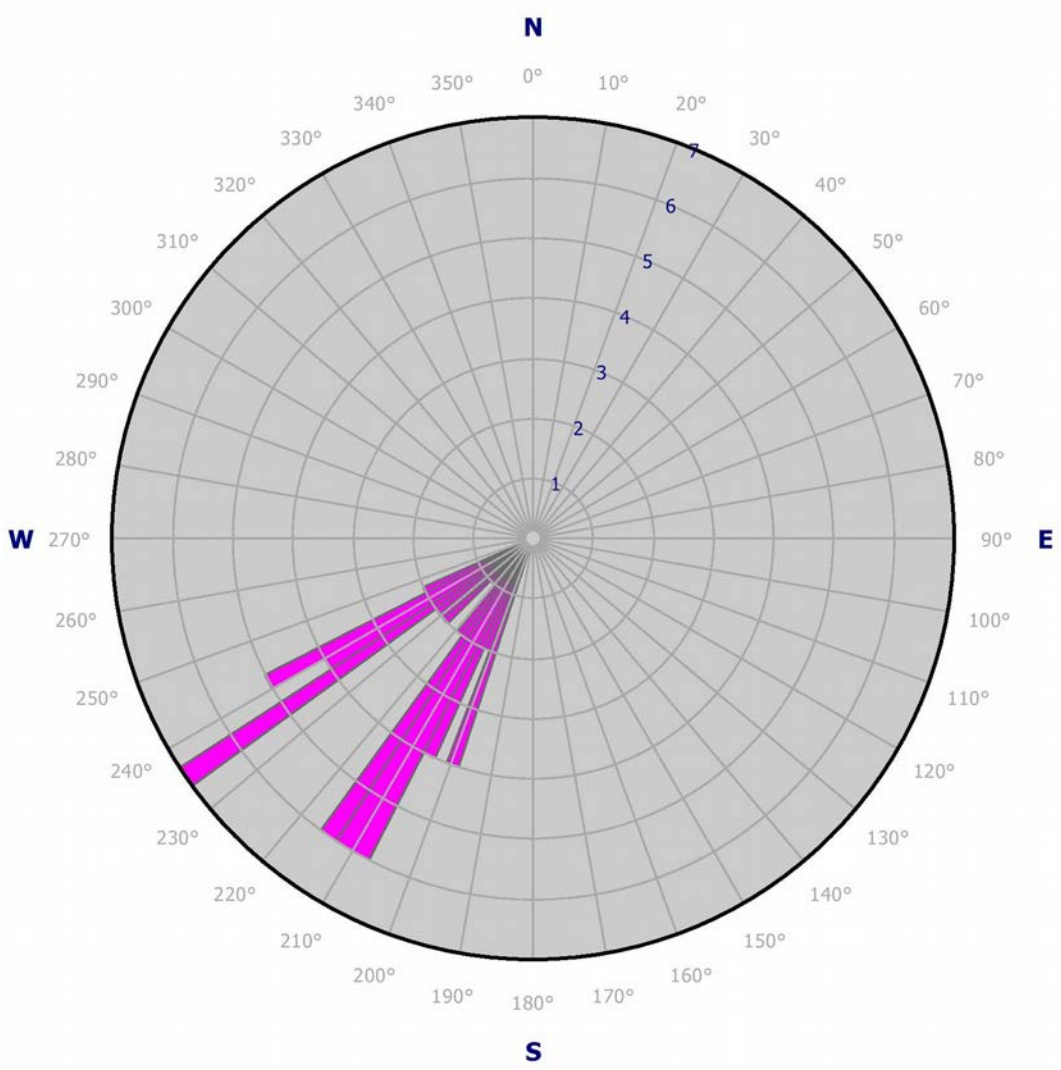

Figure 8. A rose diagram shows the ice flow direction of all the crag-and-tails mapped.

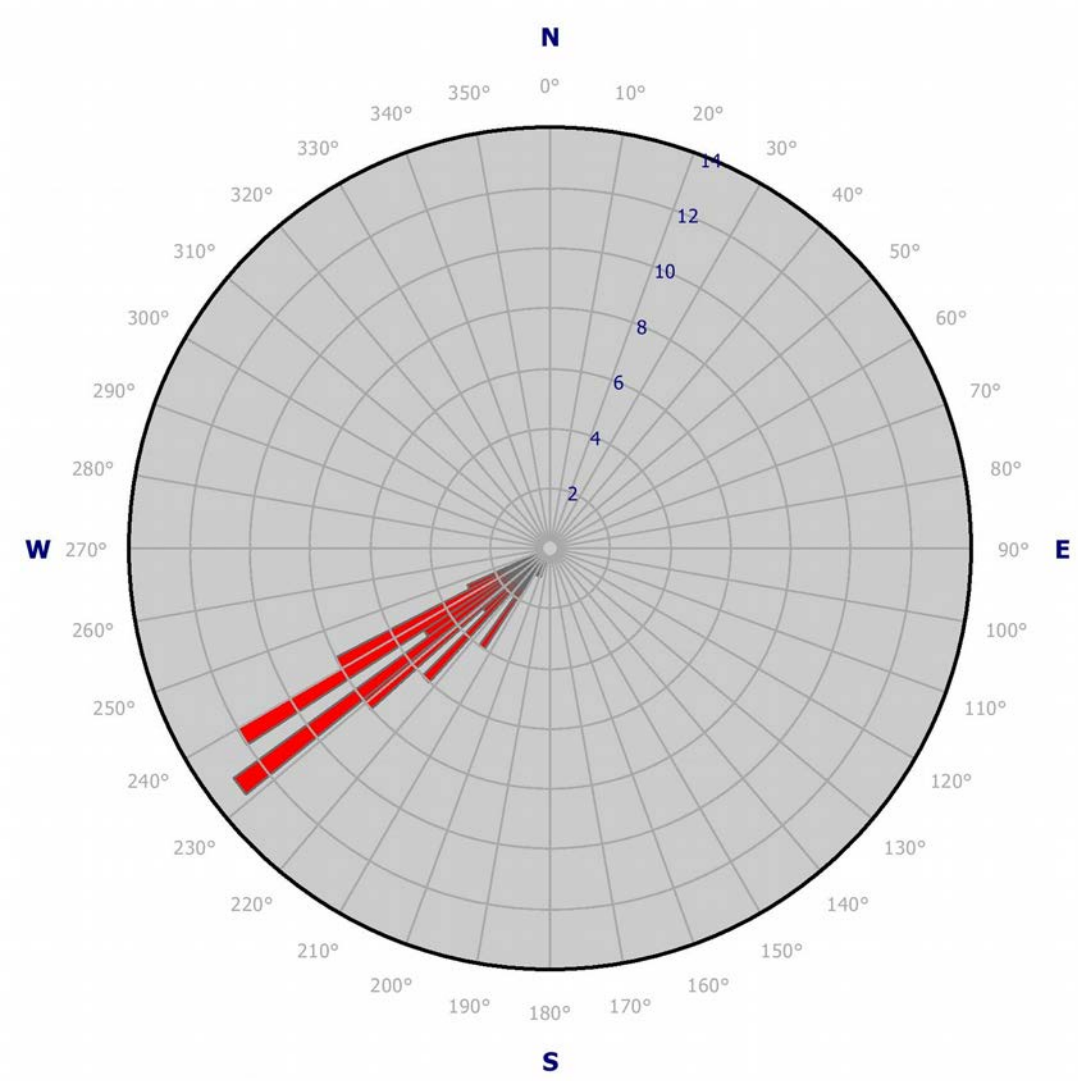

Figure 9. A rose diagram shows the ice flow direction of all the stoss-side moraines mapped.

3.3 General comments about the regional distribution of features

As can be observed in Figures 4-7, the crag-and-tails are uncommon in close proximity to the coastline, whereas the stoss-side moraines are common there. This could be because the crag-and-tails are smaller and commonly at the highest elevation in the local area, as a result they are less resistant to erosion. However, no clear trend is evident in the distribution of the streamlined till patches that do not outline a stoss-side moraine. There are almost no features towards the south-east. This is likely because the bedrock knobs in this region have been covered by sediment to a greater extent due to the lower elevation above sea level, making them impossible to map from LiDAR data alone. Features also become less common towards the north-east region which is close to the area where exposed bedrock can no longer be observed. Streamlined till patches refers to a continuous area primarily made of till that is elevated relative to its surroundings, making a clear outline visible. This till patch is often surrounded by bedrock and crag-and-tails are usually deposited on top of it. Many of them also outline the extent of stoss-side moraines.

3.4 What is the dominant ice flow direction

The dominant ice flow direction in the study area is towards the south-west. Using the average of both stoss-side moraines and crag-and-tails the true azimuth for the entire study area is 229°. In Figure 8 two trends can be seen. The crag-and-tails trending towards 210° are located towards central Sweden and those trending towards 240° are located towards the coastline. Figure 9 only shows a single trend, which can be explained by the fact that the stoss-side moraines are uncommon towards central Sweden. For more data, see Appendix A.

3.5 Profiles of stoss-side moraines

Figures 10-17 present 8 example profiles of stoss-side moraines from throughout the study area. The other 65 stoss-side moraines in the area show the same trend. One profile was purposefully selected since it has been previously studied (Hillefors, 1974). The remaining 7 profiles out of the 73 other stoss-side moraines (Profiles 2-8) were randomly selected. For all other 65 profiles, see Appendix C. All profiles shown in Figures 10-17 are drawn parallel to the ice flow direction.

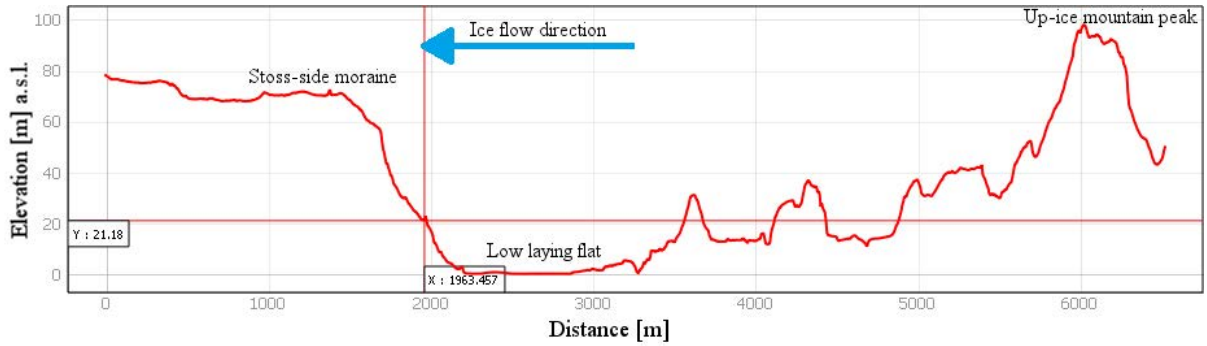

Figure 10. Illustrative profile 1 (N: 6422817 E: 324486, Dösebacka).

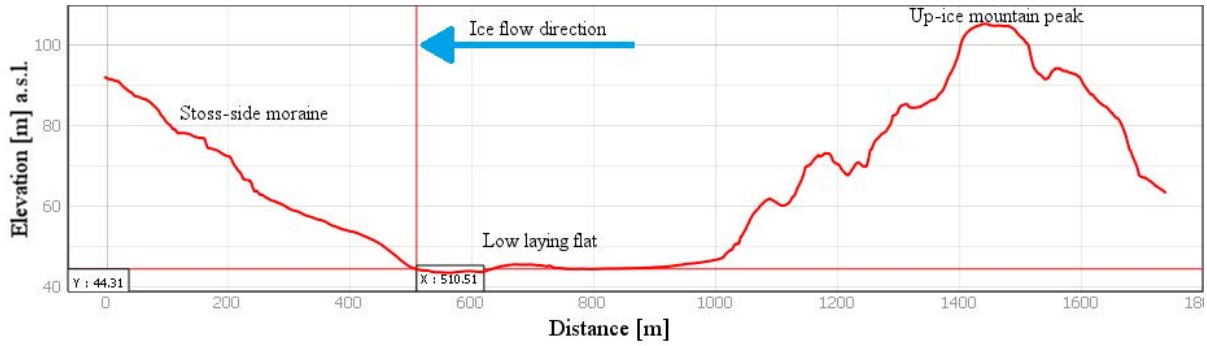

Figure 11. Illustrative profile 2 (N: 6340402 E: 345988).

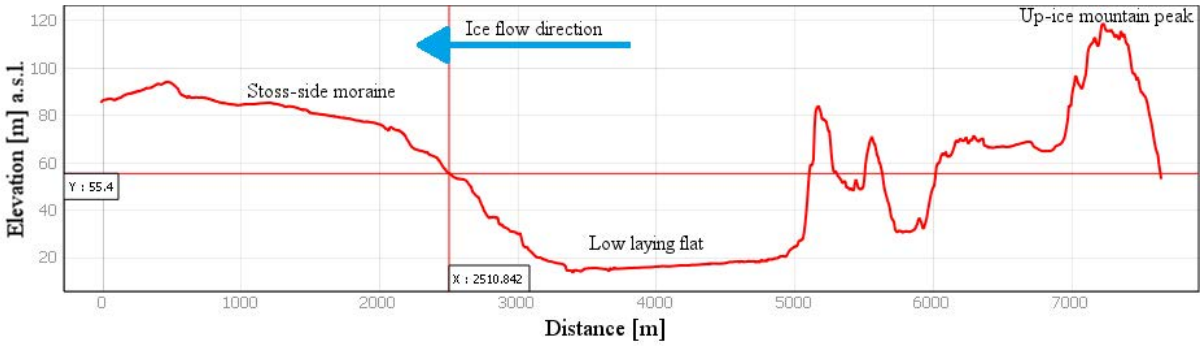

Figure 12. Illustrative profile 3 (N: 6343822 E: 343073).

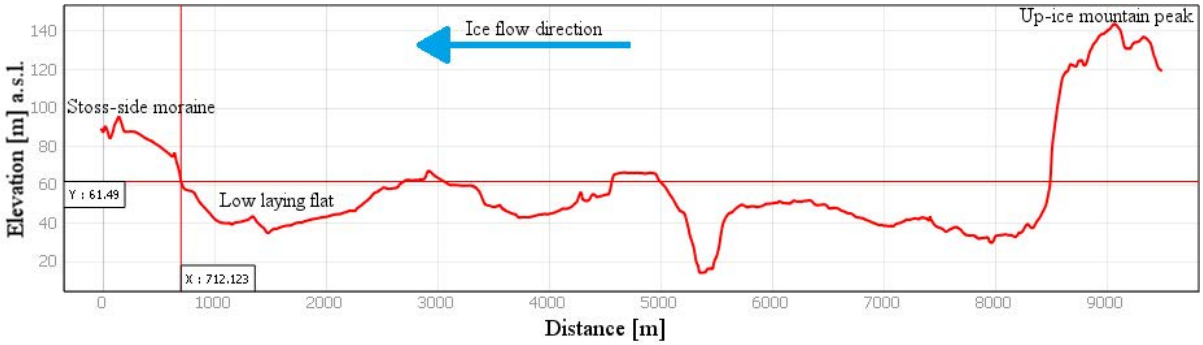

Figure 13. Illustrative profile 4 (N: 6316133 E: 353597).

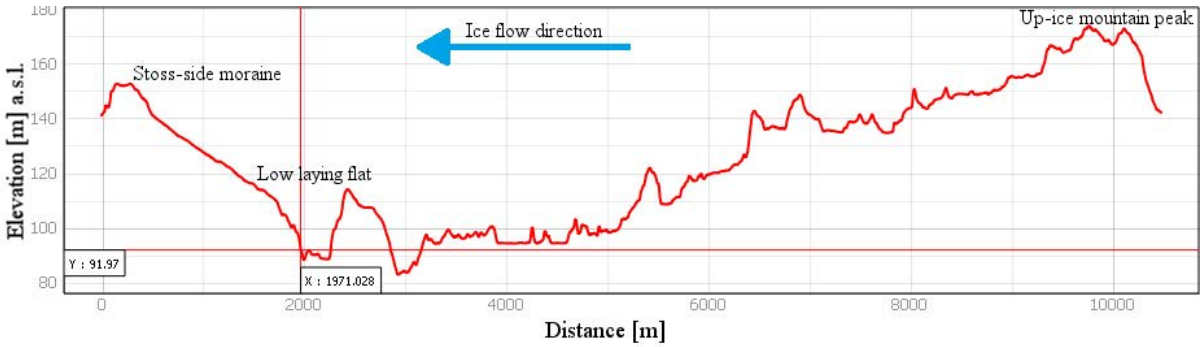

Figure 14. Illustrative profile 5 (N: 6316046 E: 363972).

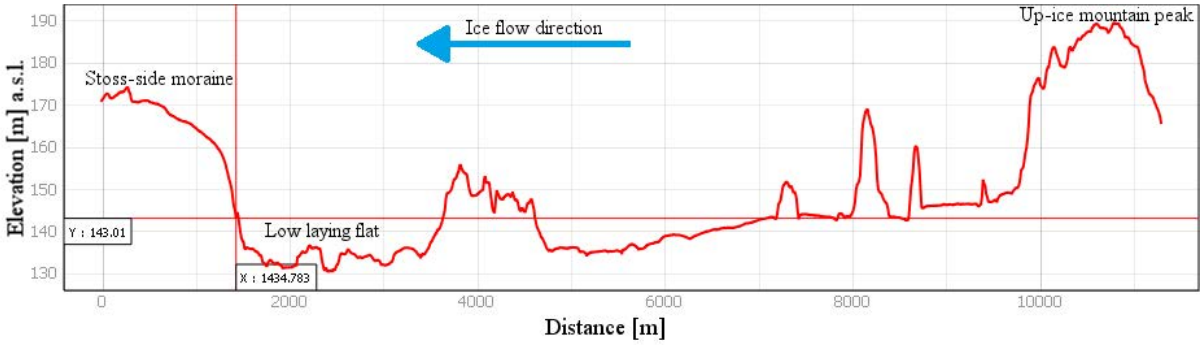

Figure 15. Illustrative profile 6 (N: 6346293 E: 382569).

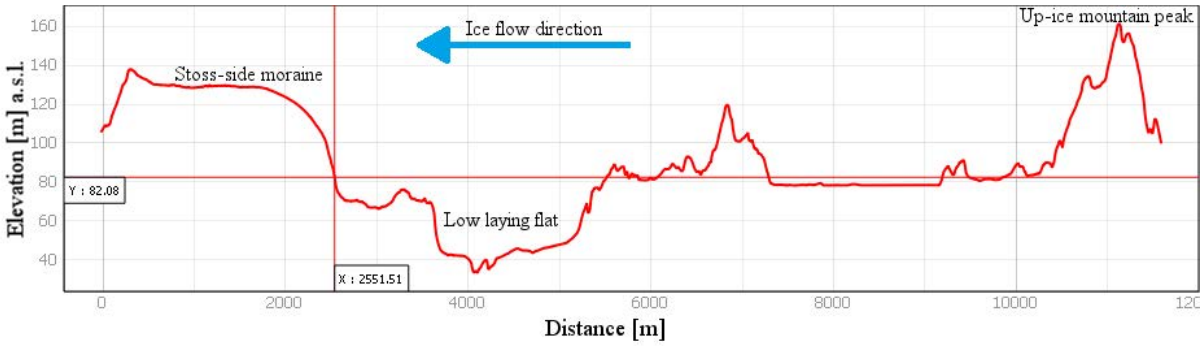

Figure 16. Illustrative profile 7 (N: 6374726 E: 349701).

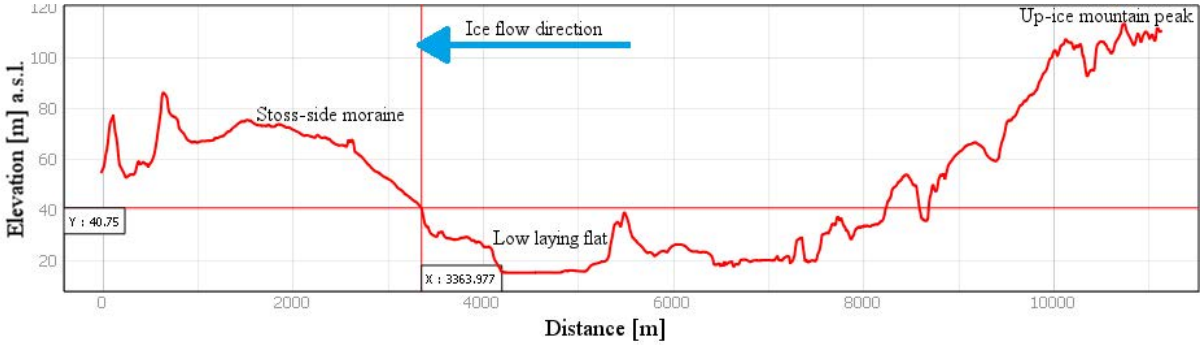

Figure 17. Illustrative profile 8 (N: 6373440 E: 334357).

The coordinate reference system for all 8 profiles is SWEREF99, i.e. EPSG:3006 and the crosshair denotes the base of the ridge. Ice flow direction to the left on the X-axis for all profiles (all units are in meters).

Figure 18 contains a bar chart of the width of the bedrock knob for all the mapped stoss-side moraines and crag-and-tails. The stoss-side moraines are sorted in ascending order and the crag-and-tails are sorted in descending order on the X-axis.

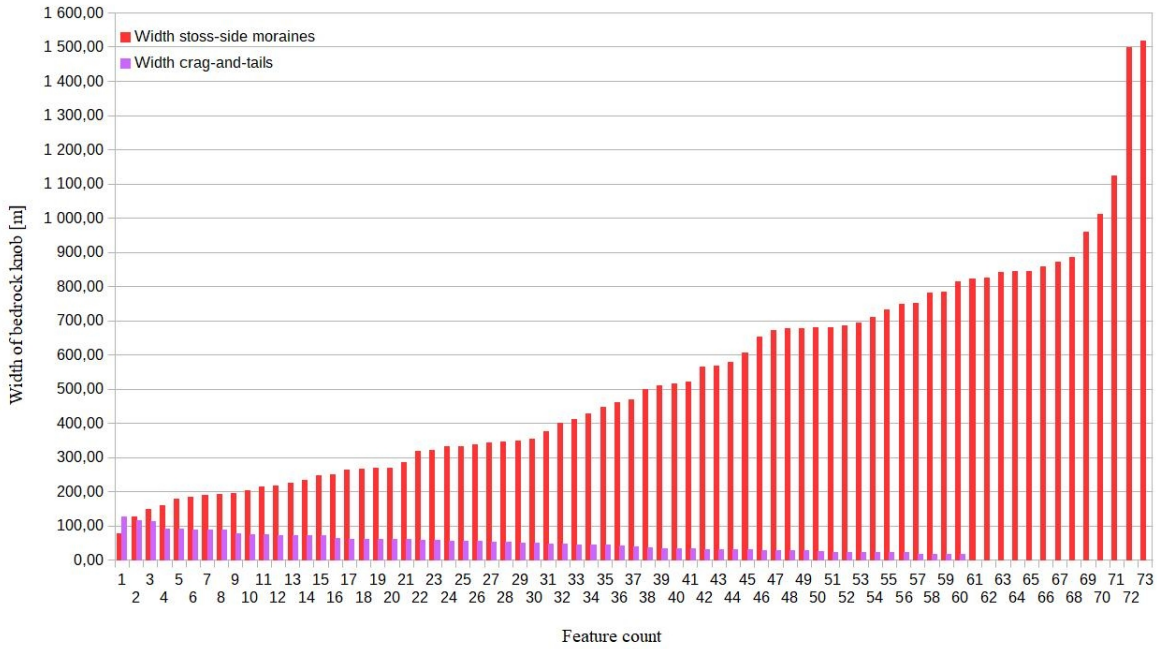

Figure 18. Width of the bedrock knobs. Width is in meters.

4. Discussion

4.1 What might explain the occurrence of stoss-side moraines

Though they vary in size, length and compass orientation there is one commonality that all stoss-side moraines share, there is always a mountain that is taller than the peak of the bedrock knob up-ice creating a sort of rock “shield” that creates an area of less glacial strain in between the mountain peaks. One reason for this pattern could be that the up-ice mountain promotes the ridge’s formation by more effectively breaking apart glacial ice, which would result in more available subglacial meltwater. This would not only help in reducing friction against the bed but also allow for more sediment to be transported in a given area. There is typically also a low laying flat in between this shield and the stoss-side moraine allowing sediment to accumulate on the stoss-side of the drumlin, as can be seen in the 8 profiles in Figures 10-17.

4.2 What might explain the two crag-and-tail trends

The two trends that can be observed in Figure 8 is explained by the topography, since all of the 33 crag-and-tails which had an azimuth of less than 220° were the most easterly ones. The westernmost of these was located at N57.180788°, E12.920898° (WGS84 crs) which is the longitude at which Sweden’s southernmost coastline starts facing west to east rather than north-north-east to south-south-east along the west coast. This aligns well with Stroeven et al. (2015) major end moraine belts where it is clear that the shape of the end moraine largely follows the shape of the land surface.

Another explanation for this ice flow direction change could be that they are of different ages, with those facing more towards the west (approximately 240°) being older. According to Hillefors (1974), there is evidence that some of the sediment in the streamlined landforms left behind by the glaciers are older than the final deglaciation of the study area which occured around 14 000 years ago (Stroeven et al., 2015). Thus, these could have formed during different stages during the glacial period, possibly with the more westerly crag-and-tails forming during the initial advance and the more easterly crag-and-tails forming later during a readvance. This is supported further by the fact that only 8 stoss-side moraines in the study area had an azimuth of less than 220° (see Figure 9 and Appendix A). Since stoss-side moraines are primarily built up before the LGM (Hillefors, 1974), it is possible that this is also the case for some crag-and-tails.

4.3 Further comments

When a stoss-side moraine was located near an old river system there was commonly a bedrock knob up-stream protecting it from erosion. Though not essential, this must have some influence on the preservation of the landform. This along with the fact that smaller till patches are common along the old river systems suggests that stoss-side moraines are plentiful wherever the topography promotes their deposition, but some of them erode away during deglaciation.

One difference between stoss-side moraines and crag-and-tails is that the bedrock knob of the stoss-side moraine is on average 526 m wide compared to crag-and-tails with an average width of 51 m, making the bedrock knob of the stoss-side moraine 10,3 times wider. From Figure 18 and Appendix D it appears as though the bedrock knobs' lower limit for a stoss-side moraine to form is approximately 80 m and the upper rock width limit for crag-and-tails appears to be approximately 130 m.

Crag-and-tails were commonly found on top of the till patches and they often appeared adjacent to other crag-and-tails, though many of these were poorly defined so they were excluded when mapping. This indicates that the crag-and-tails form wherever till can accumulate and there is a protruding bedrock knob that can allow sediment to flow in down-ice from it. Another finding was that crag-and-tails were uncommon along the coastline. The most likely explanation for this is that the crag-and-tails are both smaller and more exposed in the surrounding terrain than the stoss-side moraines and might therefore eroded away to a greater extent.

A question for future research would be to investigate the age of the sediment in crag-and-tails in order to conclude whether the crag-and-tails form at the same time in the same region. This would also confirm whether or not the landform is deposited during different glacial stages.

5. Conclusion

Based on the 8 profiles in Figures 10-17 along with the fact that all stoss-side moraines showed the same trend (see Appendix C) it is very likely that a mountain peak (here referred to as a rock shield) up-ice is a key component in the formation of stoss-side moraines, probably by generating more meltwater underneath the glacier, allowing more sediment to be transported to and within a given area. Furthermore, given how common the low laying flats are immediately up-ice from the stoss-side moraines it is likely that they are also a key component in a stoss-side moraine's formation. They are also more common along the valleys which now only contain small rivers and towards the coastline, both of which were below sea level during the LGM.

Stoss-side moraines and crag-and-tails often form in large clusters wherever their formation is promoted, which sometimes results in the landforms all merging into one. Furthermore, as can be seen in Figures 8-9 the general ice flow direction in the region shows a strong trend towards the south-west. Crag-and-tails are almost non-existent along the coastline, which suggests that most of the ones that formed there have now eroded away. The trend towards two different ice flow directions for the crag-and-tails can most likely be explained by the topography, with the land going from west to east at the same longitude as the westernmost of the low azimuth (<220°) crag-and-tails. An alternative explanation is that they are deposited at different stages of the glaciation, with the high azimuth (approximately 240°) crag-and-tails being older.

Acknowledgements

Thanks to my supervisor Mark D. Johnson for all his guidance, Alexander Walther for supplying both the DTM and the DEM TIF-files. I would also like to thank my family (Björn Lundell, Louise Lundell and Monica Lundell) for their help with reading drafts and their general support.

References

Benn, D. I. & Evans, D. J. A. (2014). *Glaciers and Glaciation.* Abingdon: Taylor and Francis.

Bouvier, V., Johnson, M. D. & Påsse, T. (2015). Distribution, genesis and annual-origin of De Geer moraines in Sweden: insights revealed by LiDAR. *GFF,* Vol. 137(4), 319-333. https://doi.org/10.1080/11035897.2015.1089933

Dowling, T. P. F., Spagnolo, M., & Möller, P. (2015). Morphometry and core type of streamlined bedforms in southern Sweden from high resolution LiDAR. *Geomorphology,* Vol. 236, 54-63. https://doi.org/10.1016/j.geomorph.2015.02.018

Engdahl, M & Påsse, T. (2014). Geologisk beskrivning av Säveåns dalgång. SGU-report 2014:37, Geological Survey of Sweden, November. Retrieved from http://resource.sgu.se/produkter/sgurapp/s1437-rapport.pdf

Gillberg, G. (1976). Drumlins in southern Sweden. *Bullettin of the Geological Institute of the University of Uppsala*, N.S., Vol. 6, pp. 125-189. Uppsala. ISSN 0302-2749

Haavisto-Hyvärinen, M. (1996). Pre-crag ridges in southwestern Finland. Sedimentary Geology, Vol. 111(3/4), 147-159. https://doi.org/10.1016/S0037-0738(97)00012-2

Hillefors, Å. (1973). The stratigraphy and genesis of stoss-and lee-side moraines, *Bulletin of the Geological Institutions of the University of Uppsala*, New Series, Vol. 5, pp. 139-154.

Hillefors, Å. (1974). The stratigraphy and genesis of the Dösebackaand Ellesbo drumlins. A contribution to the knowledge of the Weichselglacial history inwestern Sweden. *Geologiska Föreningen i Stockholm Förhandlingar,* Vol. 96(4), 355-373. https://doi.org/10.1080/11035897409454289

Howat, I. M., Ahn, Y., Joughin, I., van den Broeke, M. R., Lenaerts, J. T. M. & Smith, B. (2011). Mass balance of Greenland's three largest outlet glaciers, 2000–2010. *Geophysical research letters,* Vol. 38(12), 1-5. https://doi.org/10.1029/2011GL047565

Johnson, M. D., Schomacker, A., Benediktsson, Í. Ö., Geiger, A. J. & Ferguson, A. Active drumlin field revealed at the margin of Múlajökull, Iceland: A surge-type glacier. *Geology,* Vol. 38(10), 943-946. https://doi.org/10.1130/G31371.1

Lantmäteriet. (2020). *Elevation data, grid 2+.* Retrieved from https://www.lantmateriet.se/en/maps-and-geographic-information/geodataprodukter/produktlista/elevation-data-grid-2/#steg=1 [Accessed 5 June 2020].

Marshak, S. (2015). *Earth portrait of a planet.* 5th edition. New York: W.W. Norton & Company.

Påsse, T. (1998). Early Weichselian interstadial deposits within the drumlins at Skrea and Vinberg, southwestern Sweden. *GFF*, Vol. 120(4), 349-356. https://doi.org/10.1080/11035899801204349

SGU. (2020). *Jordarter 1:1 miljon*. Geological Survey of Sweden. Retrieved from https://apps.sgu.se/kartvisare/kartvisare-jordarter-1-miljon.html?zoom=326427.3742860551,6374362.479352118,369435.4603022272,6393934.518496197 [Accessed 5 June 2020].

Smith, A. M., Murray, T., Nicholls, K. W., Makinson, K., Adalgeirsdóttir, G., Behar, A. E. & Vaughan, D. G. (2007). Rapid erosion, drumlin formation, and changing hydrology beneath an Antarctic ice stream. *Geology*, Vol. 35(2), 127-130. https://doi.org/10.1130/G23036A.1

Stearns, L. A. & Hamilton. G. S. (2007). Rapid volume loss from two East Greenland outlet glaciers quantified using repeat stereo satellite imagery. *Geophysical research letters*, Vol. 34(5), 1-5. https://doi.org/10.1029/2006GL028982

Steiniger, S. & Bocher, E. (2009). An overview on current free and opensource desktop GIS developments. *International Journal of Geographical Information Science,* Vol. 23(10), 1345-1370. https://doi.org/10.1080/13658810802634956

Stroeven, A. P., Hättestrand, C., Kleman, J., Heyman, J., Fabel, D., Fredin, O. & ... Jansson, K. N. (2015). Deglaciation of Fennoscandia. *Quaternary Science Reviews,* Vol. 147, 91-121. https://doi.org/10.1016/j.quascirev.2015.09.016

Appendix A: All metadata from the maps

Length crag-and-tails [m]	x coordinate crag-and-tails	y coordinate crag-and-tails	Azimuth crag-and-tails	Azimuth stoss-side moraines	x coordinate stoss-side moraine	y coordinate stoss-side moraine
54,40	395 589,04	6 363 188,76	200	202	387 350,15	6 354 676,73
326,40	398 043,25	6 373 580,95	200	207	389 996,73	6 384 944,36
197,90	390 573,61	6 367 388,21	202	214	351 427,59	6 439 531,70
267,00	399 016,29	6 377 421,70	202	215	347 932,63	6 360 020,71
133,40	389 206,83	6 397 720,65	204	215	382 569,13	6 346 293,41
147,20	396 405,94	6 362 371,20	204	216	356 942,85	6 331 926,35
125,00	397 038,76	6 342 666,08	206	217	394 519,46	6 361 961,75
142,20	395 121,39	6 362 041,13	206	218	393 914,89	6 361 773,24
126,10	395 463,36	6 362 866,63	207	220	379 824,31	6 388 303,42
164,50	394 900,51	6 383 794,49	207	223	336 412,03	6 342 884,44
290,70	397 086,49	6 387 597,41	209	224	353 900,02	6 352 993,89
85,90	394 922,29	6 361 885,69	210	224	392 397,23	6 391 514,14
197,80	395 835,76	6 363 061,76	210	225	388 564,45	6 385 961,81
322,20	396 663,85	6 365 531,13	210	226	336 320,96	6 366 100,66
623,10	396 139,97	6 363 980,67	210	226	349 155,40	6 352 048,99
74,70	394 035,28	6 361 446,48	211	227	343 073,43	6 343 822,63
100,10	395 180,26	6 362 027,90	211	228	381 052,86	6 368 994,04
447,90	382 109,49	6 345 066,92	211	229	344 960,98	6 340 766,49
179,00	393 270,29	6 382 555,03	212	229	353 814,23	6 329 915,50
205,80	396 520,37	6 362 644,38	212	229	341 747,32	6 384 929,70
224,00	388 845,61	6 337 432,66	212	230	354 511,40	6 328 863,78
704,70	395 985,19	6 364 027,63	212	230	349 577,36	6 407 254,04
89,60	393 813,69	6 361 406,13	213	230	336 016,77	6 341 621,08
94,40	397 307,37	6 329 530,39	213	230	376 452,13	6 390 064,81
458,40	396 293,43	6 363 970,09	213	231	345 201,75	6 341 782,49
312,70	378 273,12	6 339 560,74	215	231	354 908,66	6 327 471,04
209,20	374 885,64	6 339 010,55	216	232	345 988,22	6 340 402,02
507,20	374 486,12	6 339 367,74	216	232	381 542,55	6 369 859,84
221,80	390 216,90	6 376 475,78	217	232	353 597,00	6 316 133,25
345,20	374 323,40	6 339 427,27	217	233	334 357,75	6 373 440,20
287,10	380 046,87	6 311 306,52	219	233	349 760,55	6 355 413,44
1 045,00	385 697,50	6 315 219,77	219	233	346 901,46	6 371 876,71
211,00	377 251,67	6 341 420,44	220	233	346 003,98	6 341 383,13

144,10	371 097,10	6 373 605,26	225	234	346 379,14	6 342 602,03
101,50	345 188,44	6 340 725,42	227	234	351 891,96	6 331 423,64
165,20	349 494,52	6 397 410,71	230	234	355 265,21	6 330 102,54
546,20	369 978,74	6 377 862,59	231	234	339 144,84	6 383 032,76
318,70	359 450,97	6 380 150,57	233	235	355 593,93	6 325 379,51
261,60	350 441,38	6 379 203,59	234	235	349 690,58	6 434 116,82
286,00	374 578,44	6 423 118,13	235	235	354 816,11	6 410 792,85
228,30	352 958,68	6 320 315,21	236	235	324 486,63	6 422 817,55
255,40	351 740,57	6 377 753,84	237	236	339 904,93	6 357 944,59
387,40	351 599,20	6 319 636,40	237	236	341 733,92	6 340 970,66
566,00	346 091,57	6 359 135,73	237	237	322 740,38	6 418 776,04
274,40	361 567,52	6 307 058,38	239	238	363 029,67	6 294 733,03
305,70	353 217,35	6 352 854,58	239	238	361 518,85	6 311 707,92
305,70	354 299,80	6 318 116,44	239	238	355 804,80	6 381 444,86
331,90	361 473,06	6 307 127,83	239	239	346 239,58	6 342 267,34
444,80	363 608,21	6 298 350,17	239	239	331 760,51	6 428 287,78
300,10	357 990,13	6 368 838,07	240	239	354 619,06	6 318 273,22
321,90	354 364,79	6 317 939,77	241	239	362 400,78	6 310 474,41
188,60	345 148,31	6 358 485,66	242	240	344 249,11	6 358 516,14
197,90	348 534,23	6 436 831,37	243	240	357 261,84	6 377 263,53
582,70	348 812,04	6 436 888,25	243	240	367 089,12	6 292 307,25
281,70	348 318,59	6 436 893,55	244	241	352 686,16	6 323 967,95
789,80	348 453,53	6 436 572,08	244	241	351 021,41	6 333 257,60
390,60	348 166,46	6 436 546,94	245	241	321 678,40	6 416 695,46
1 423,60	336 066,51	6 353 283,15	245	241	349 701,71	6 374 726,56
257,50	348 452,37	6 372 380,65	247	241	322 923,46	6 381 894,36
545,20	343 659,48	6 368 826,04	247	242	322 794,24	6 423 686,87
				242	341 654,77	6 365 446,02
				242	365 239,06	6 427 101,37
				242	358 943,09	6 369 313,38
				243	354 337,64	6 437 178,23
				243	349 242,38	6 436 943,83
				243	358 438,12	6 296 145,54
				244	344 550,14	6 368 958,19
				244	345 154,12	6 342 025,24
				244	363 972,97	6 316 046,11

				246	356 401,02	6 368 779,47
				246	330 241,98	6 414 777,53
				247	319 391,07	6 418 112,31
				249	358 381,13	6 296 415,55

Table A:1. All metadata from the map. Length in meters, azimuth is in degrees clockwise rotation from true north and all coordinates are listed using the SWEREF99, i.e. EPSG:3006 map projection.

Appendix B: Detailed map sections

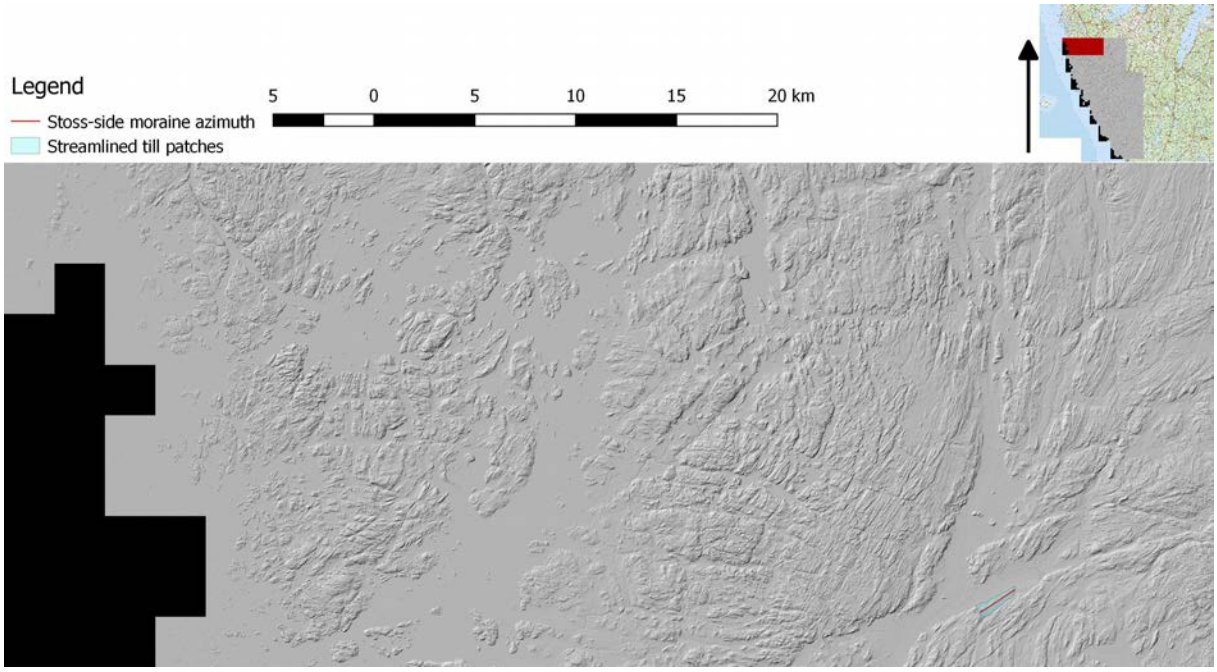

Figure B:1. Distribution of features in sector 09B009.

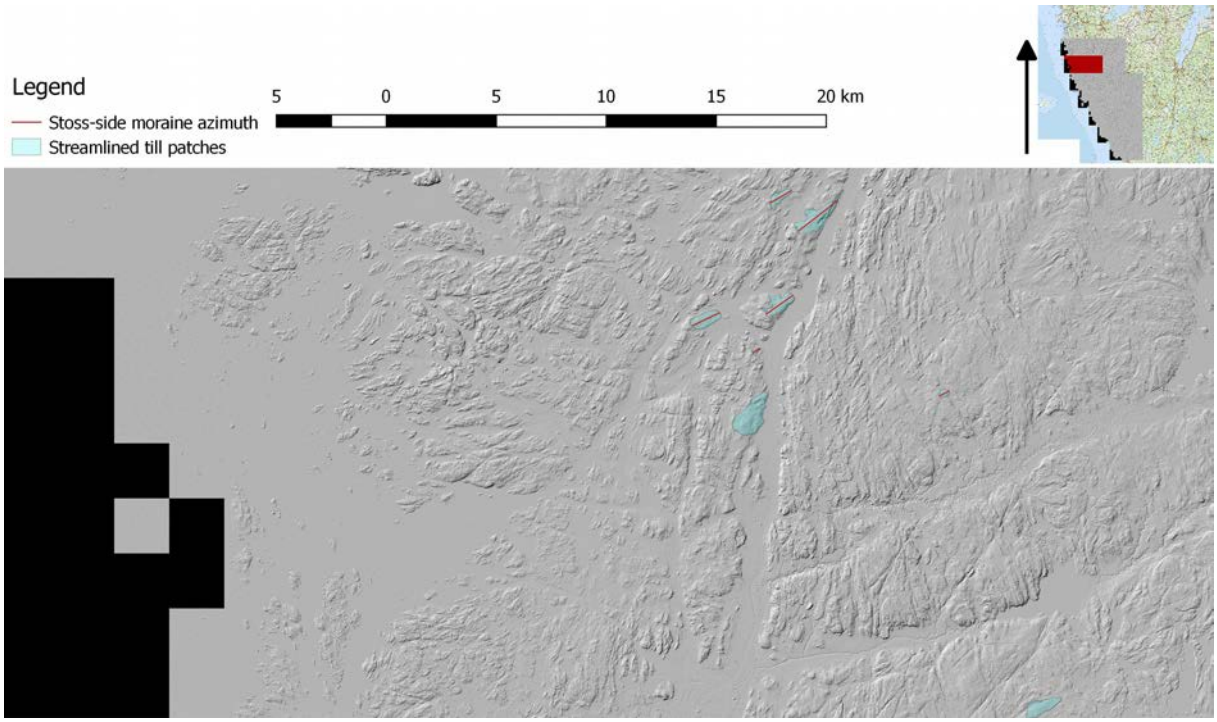

Figure B:2. Distribution of features in sector 09B008.

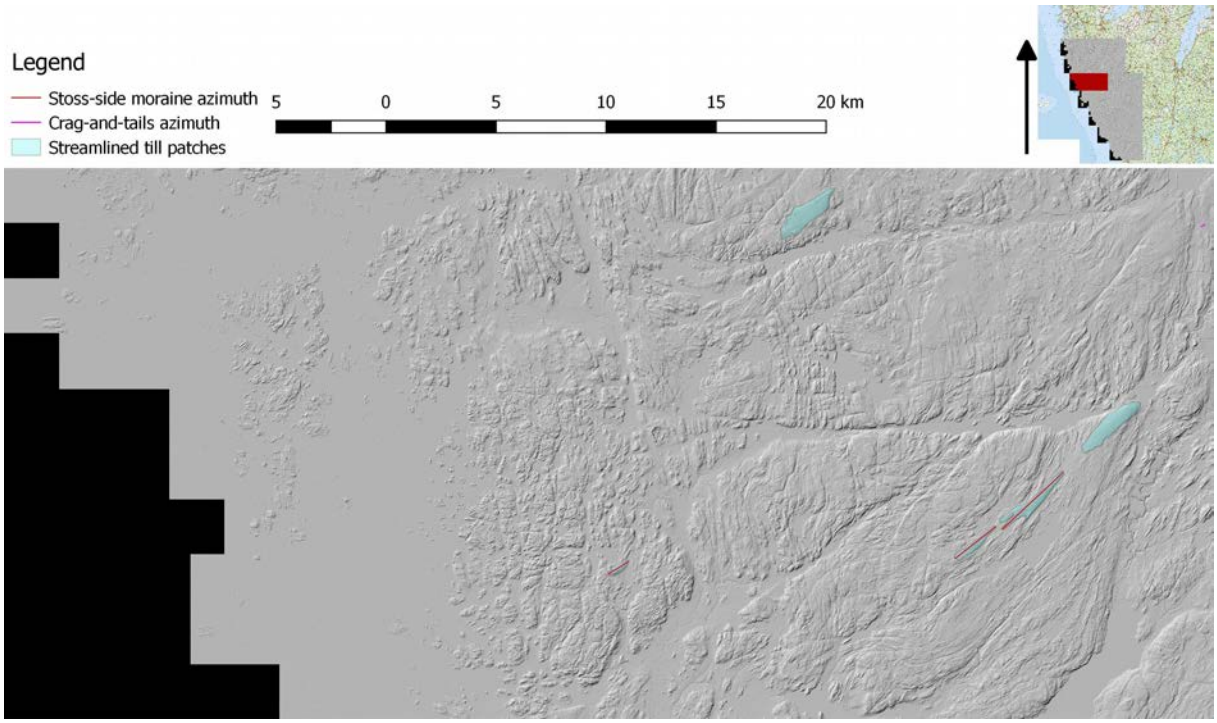

Figure B:3. Distribution of features in sector 09B002.

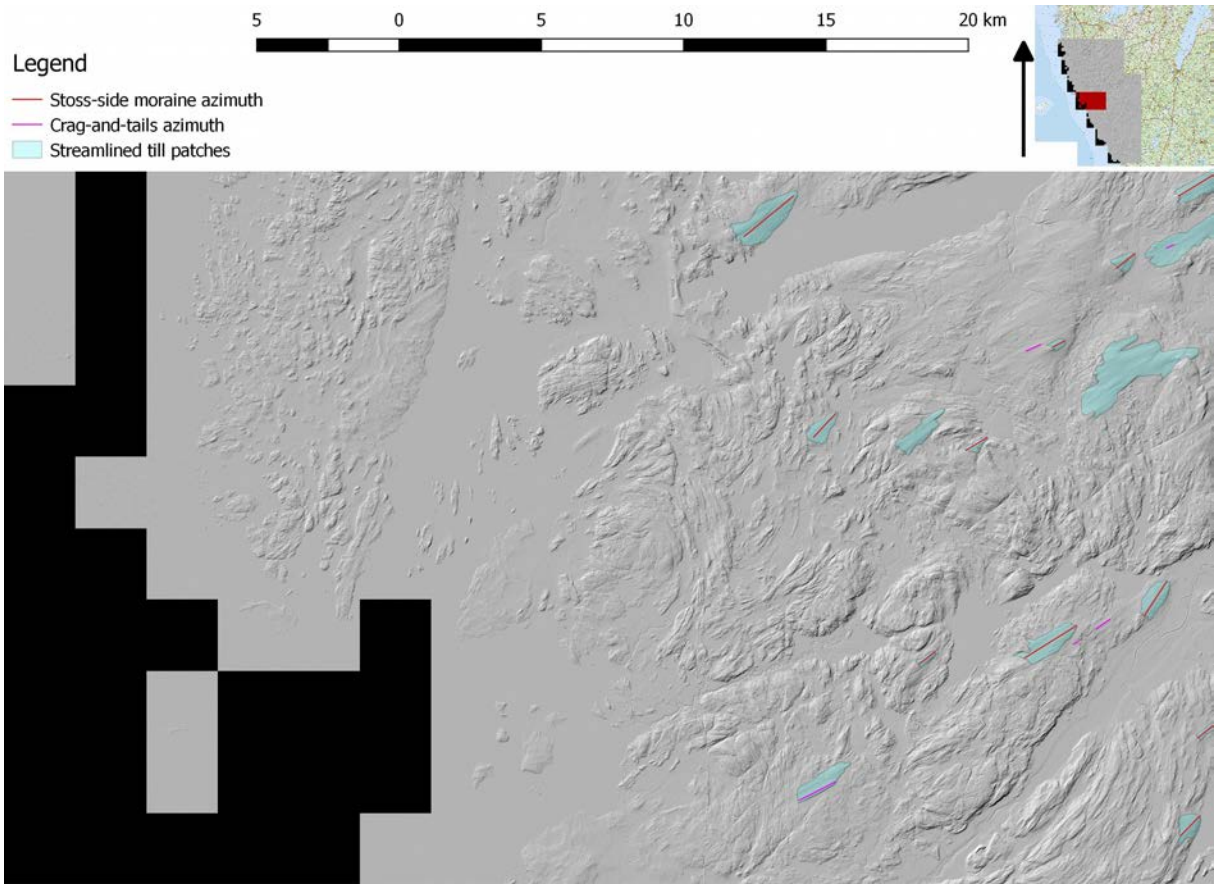

Figure B:4. Distribution of features in sector 09B001.

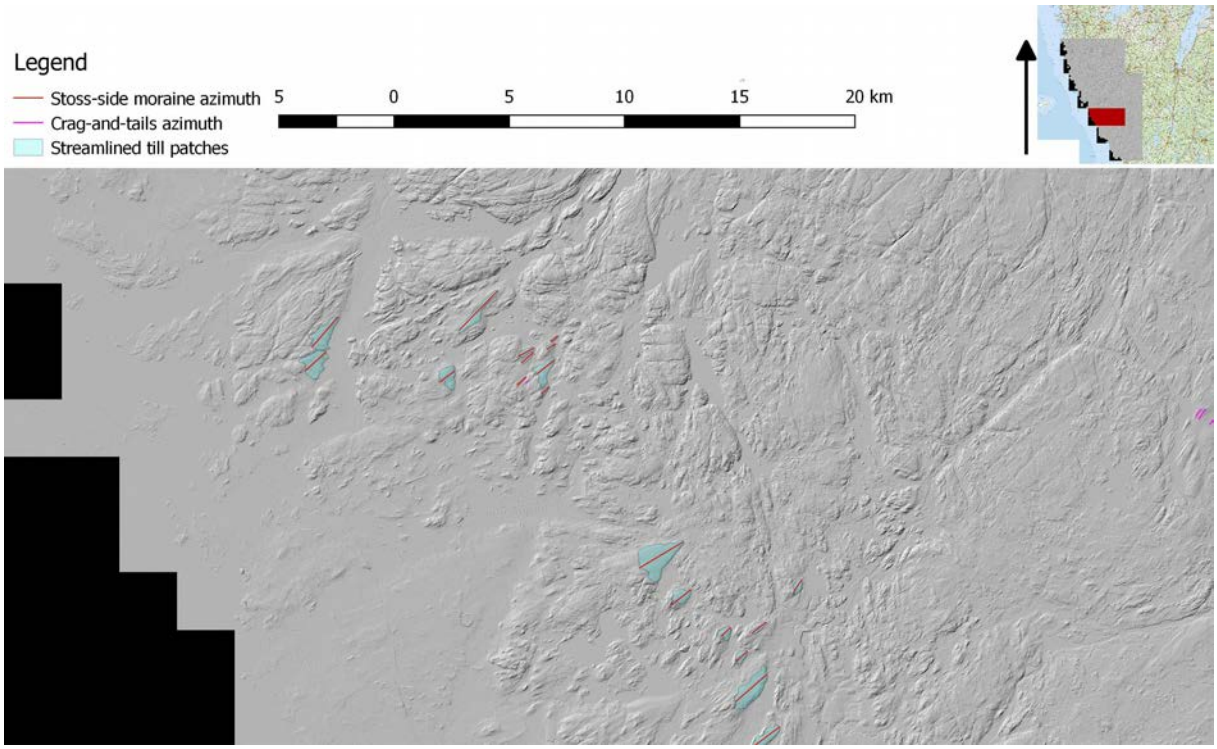

Figure B:5. Distribution of features in sector 10A030.

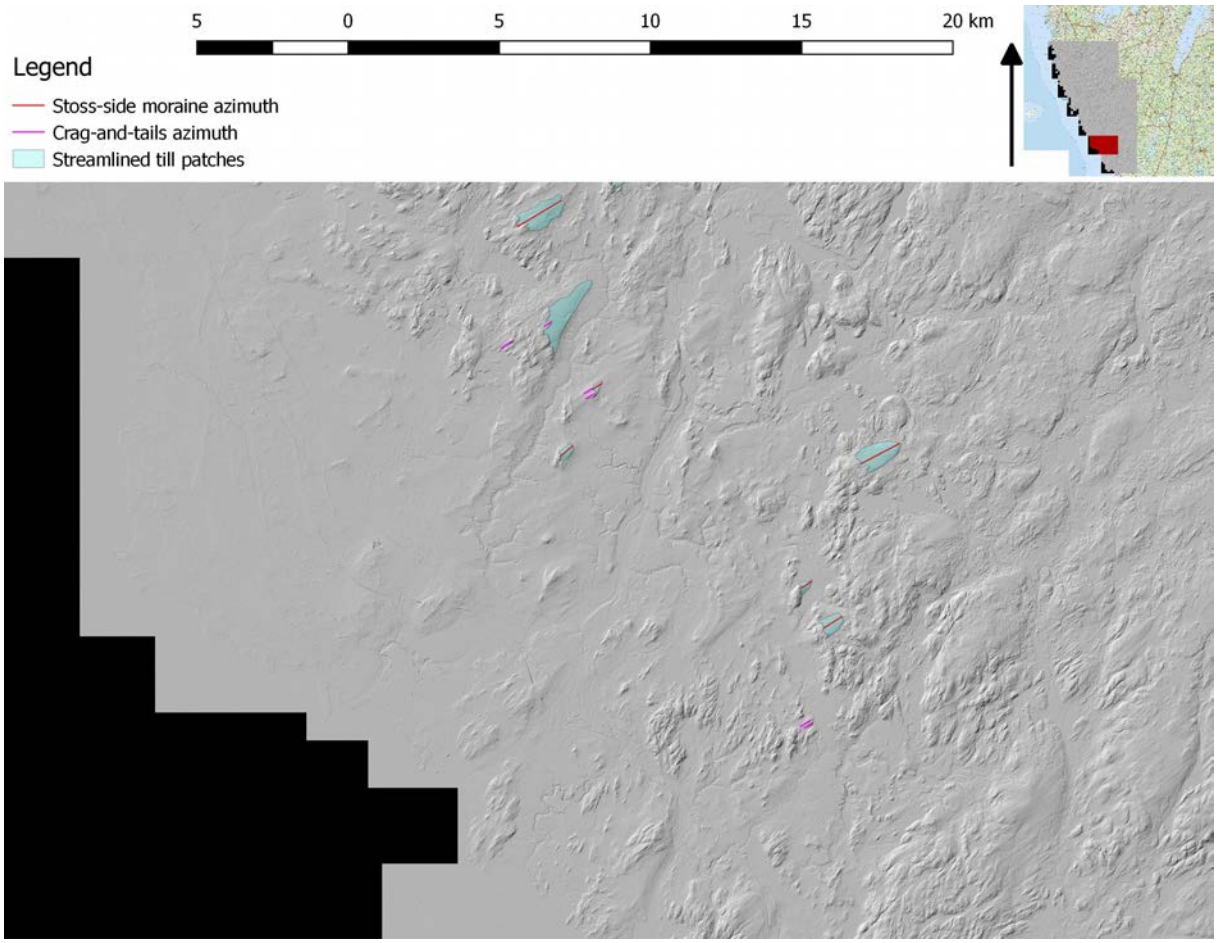

Figure B:6. Distribution of features in sector 10A029.

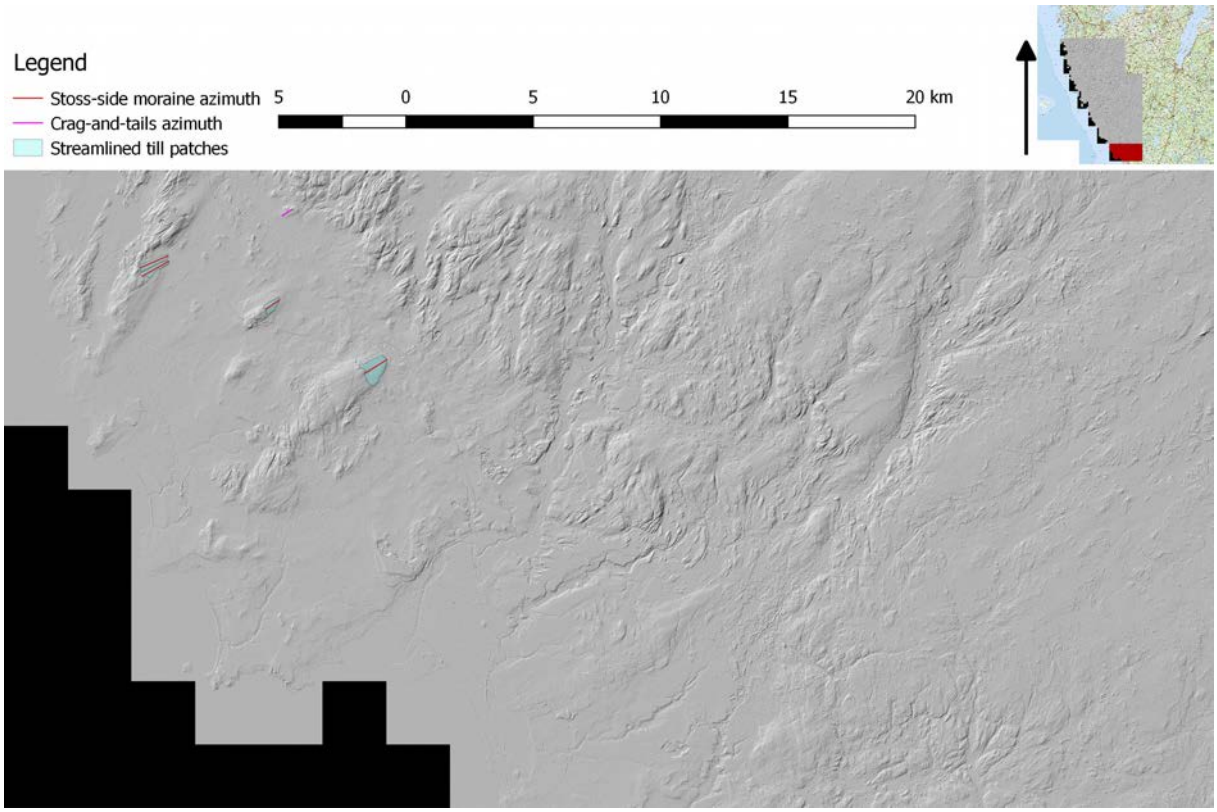

Figure B:7. Distribution of features in sector 10A012.

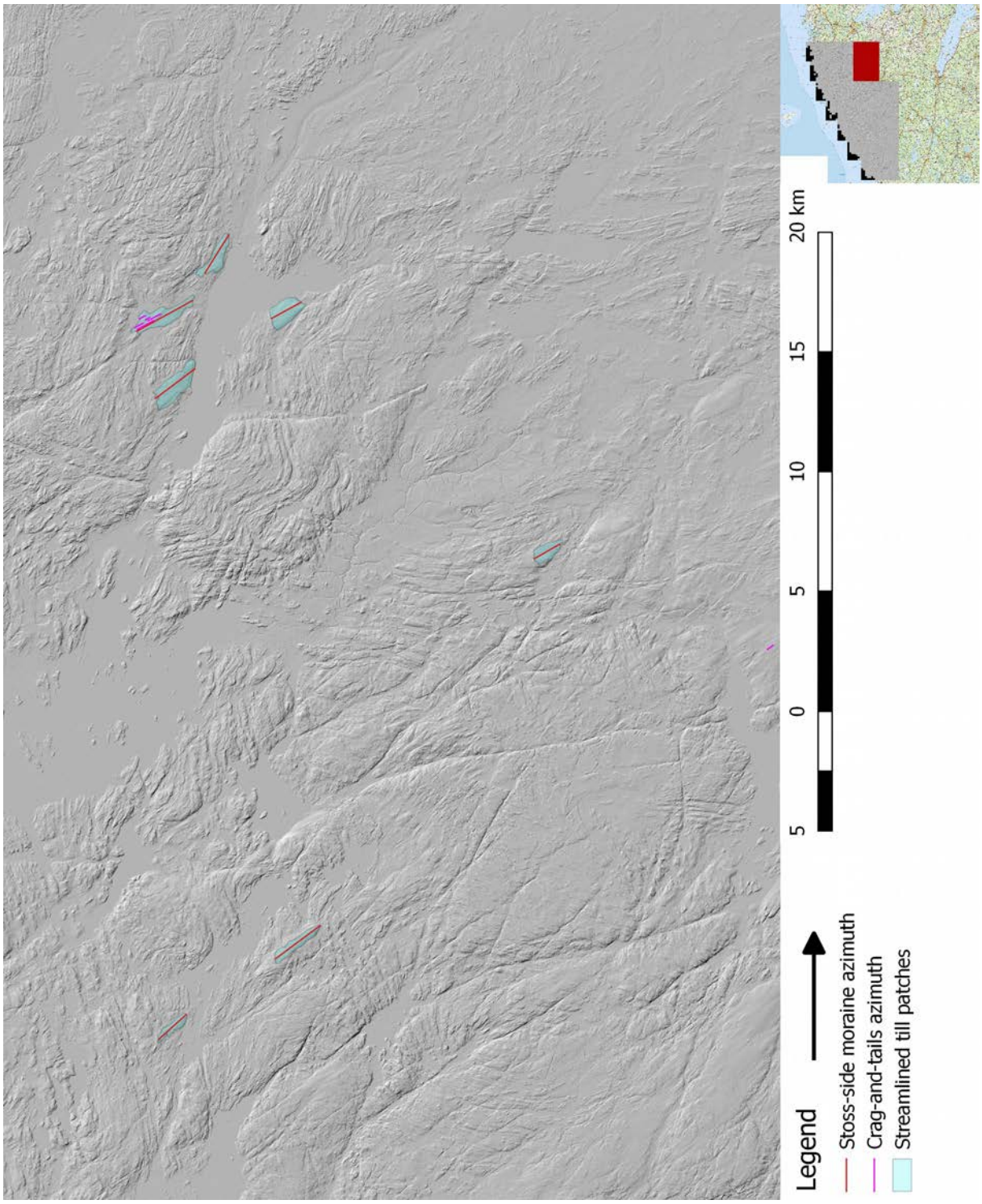

Figure B:8. Distribution of features in sector 09B010.

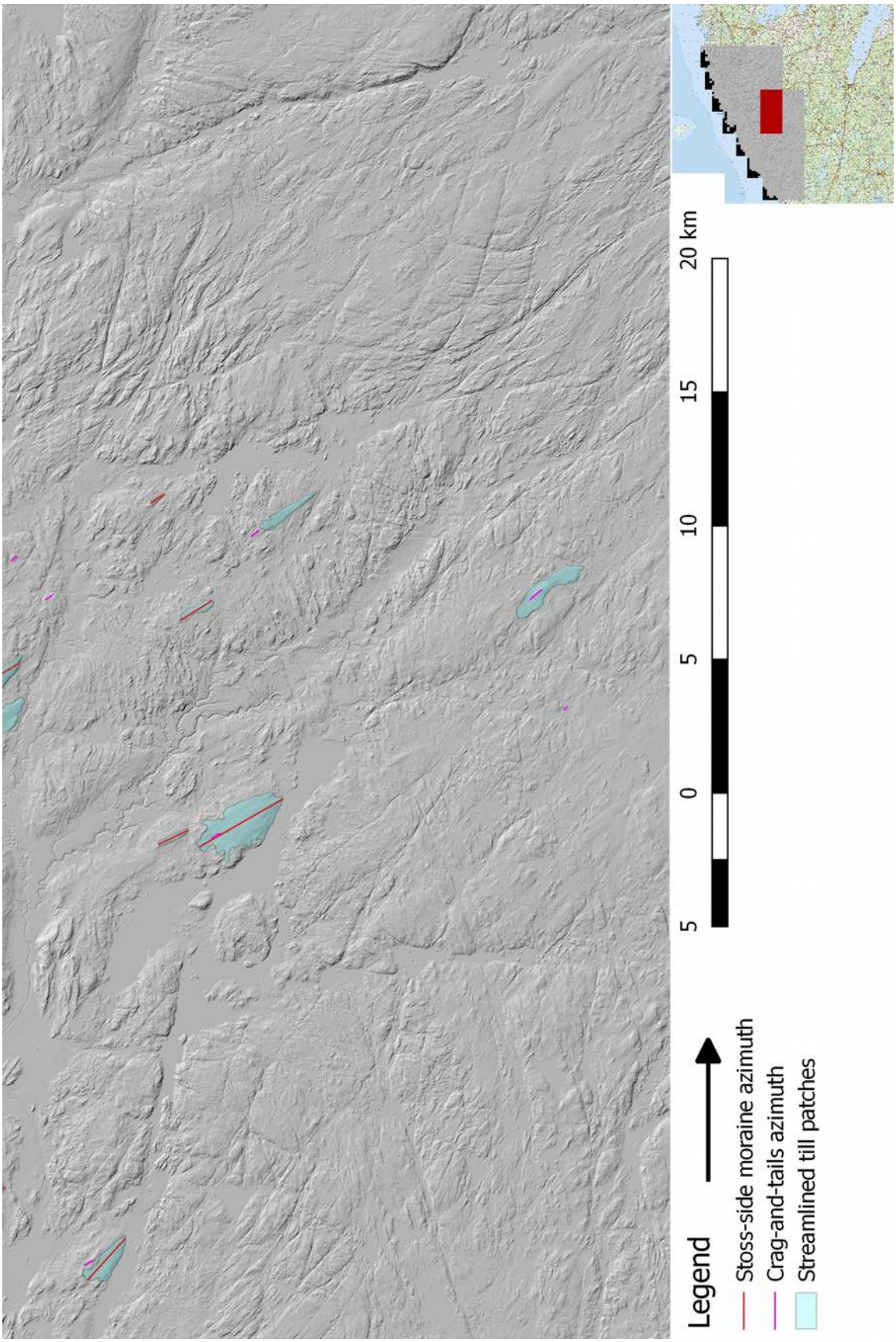

Figure B:9. Distribution of features in sector 09B003.

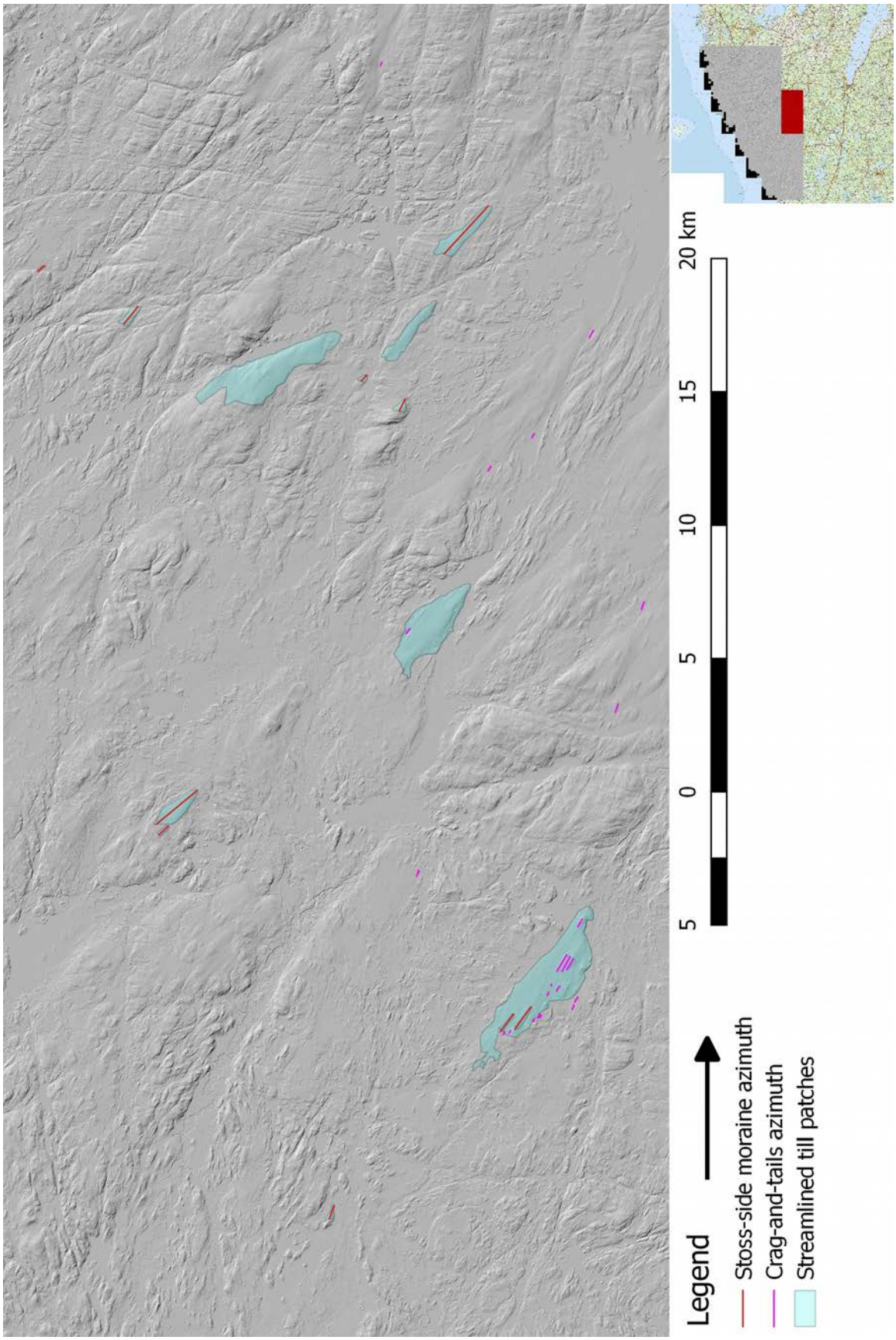

Figure B:10. Distribution of features in sector 09B004.

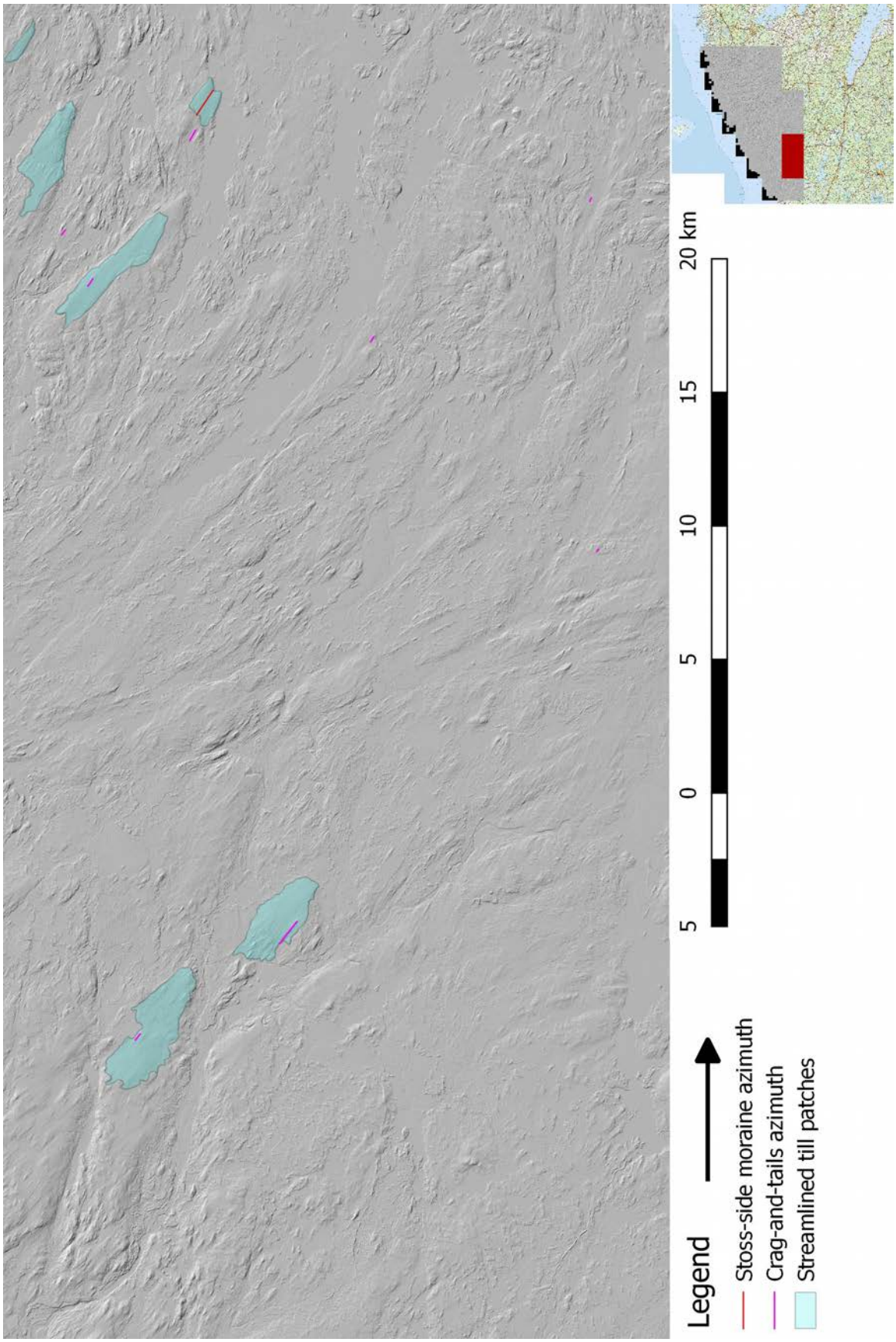

Figure B:11. Distribution of features in sector 10A031.

Appendix C: Profiles for the remaining 65 profiles

All coordinates (see Figures C:1-C:65) are listed using the SWEREF99, i.e. EPSG:3006 map projection. Some profiles extend beyond the furthest down-ice side of the stoss-side moraines. Ice flow direction to the left on the X-axis for all profiles. The units on both the X and the Y axis are in meters.

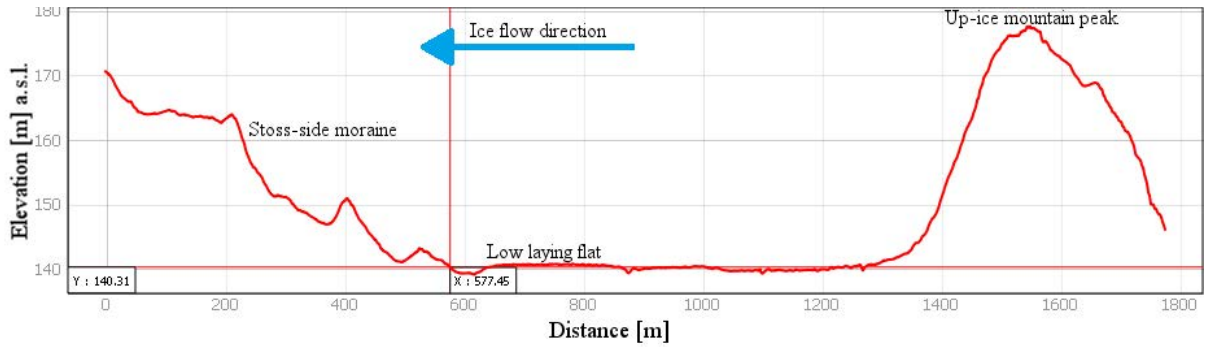

Figure C:1. Profile of the stoss-side moraine located at (N: 6354676 E: 387350).

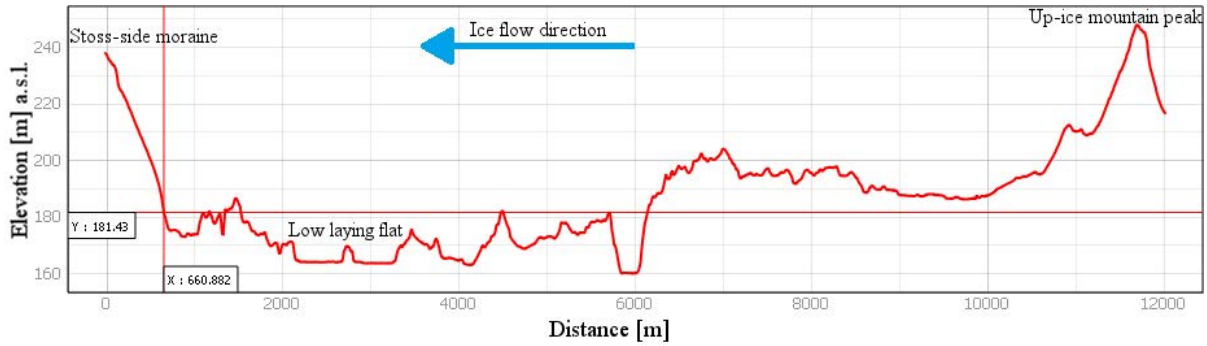

Figure C:2. Profile of the stoss-side moraine located at (N: 6361773 E: 393915).

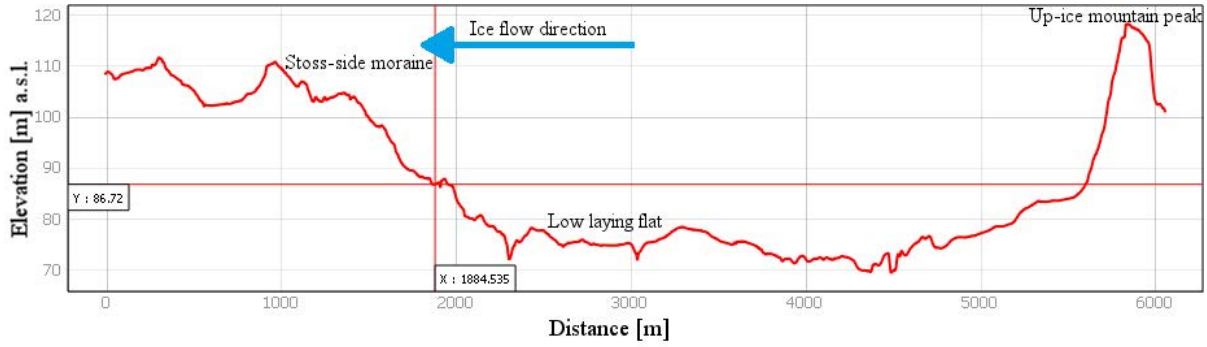

Figure C:3. Profile of the stoss-side moraine located at (N: 6439531 E: 351427).

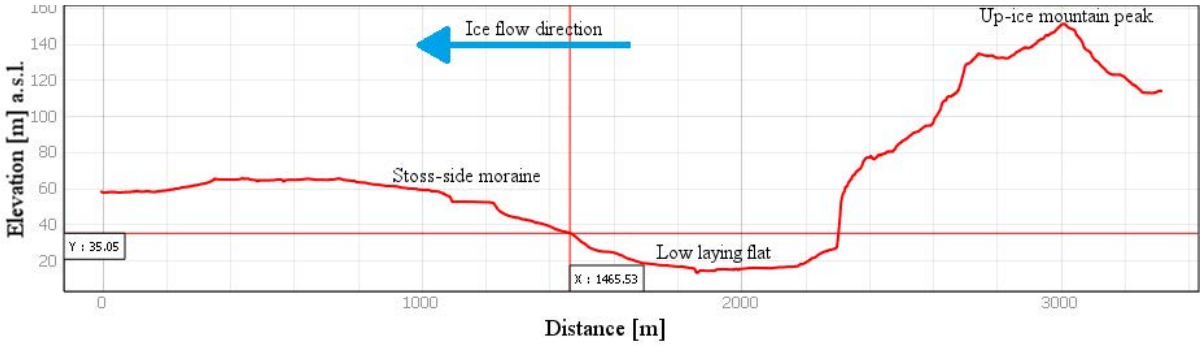

Figure C:4. Profile of the stoss-side moraine located at (N: 6360020 E: 347932).

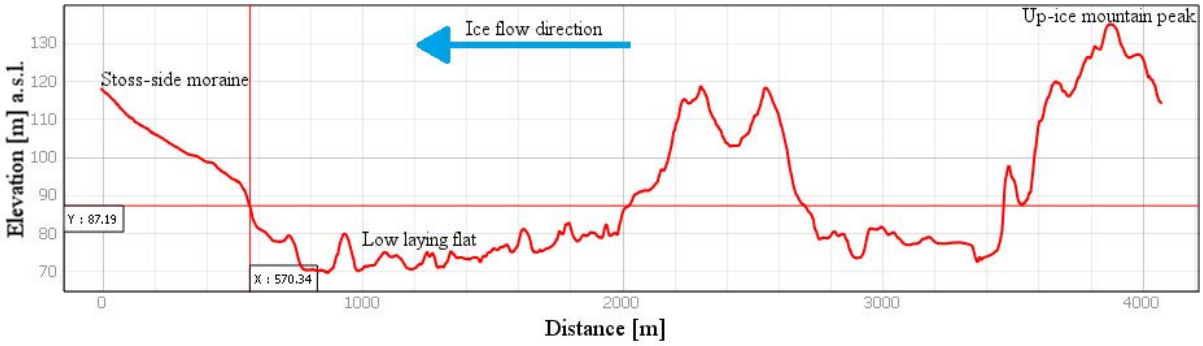

Figure C:5. Profile of the stoss-side moraine located at (N: 6331926 E: 356942).

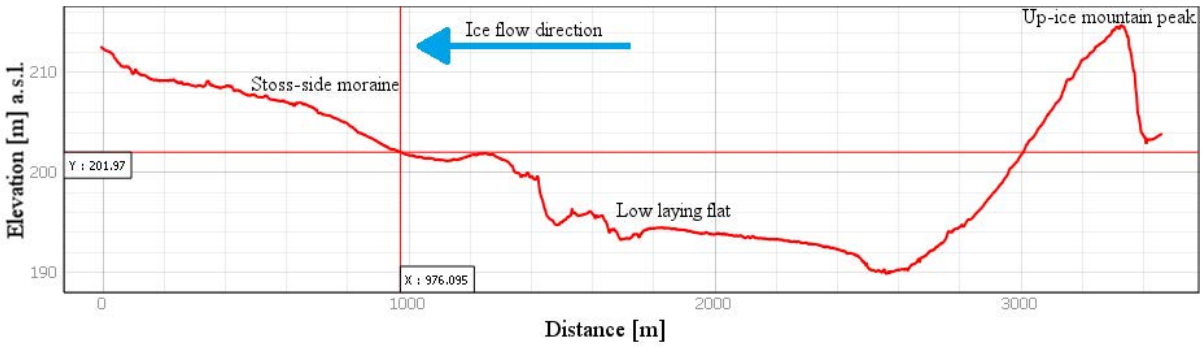

Figure C:6. Profile of the stoss-side moraine located at (N: 6361961 E: 394519).

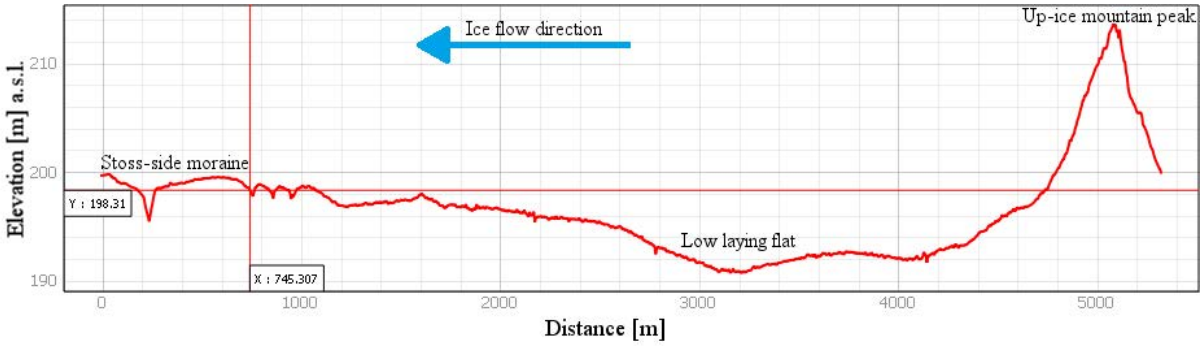

Figure C:7. Profile of the stoss-side moraine located at (N: 6361773 E: 393914).

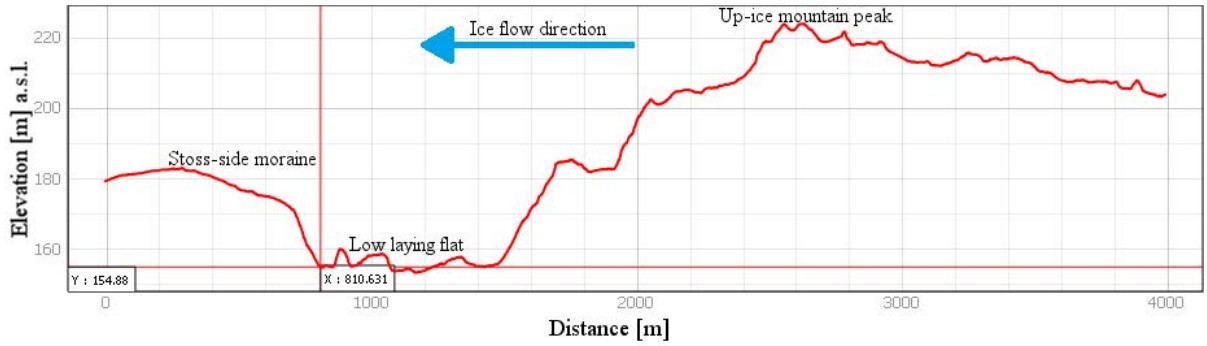

Figure C:8. Profile of the stoss-side moraine located at (N: 6388303 E: 379824).

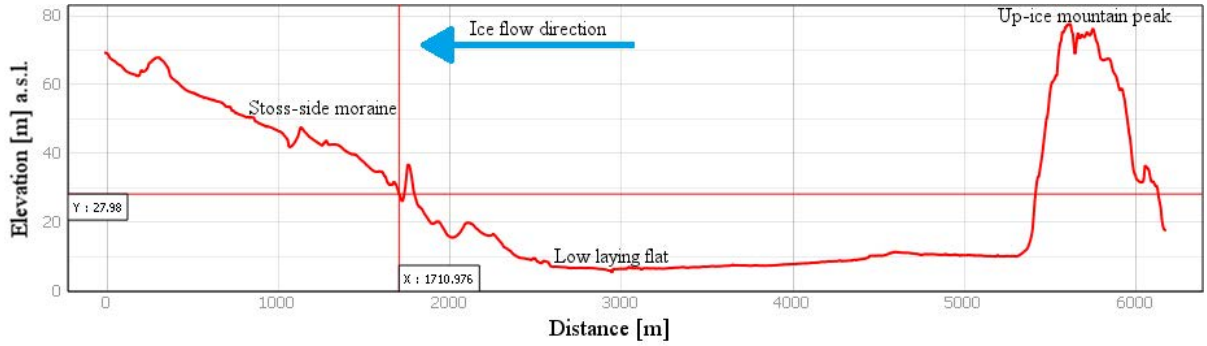

Figure C:9. Profile of the stoss-side moraine located at (N: 6342884 E: 336412).

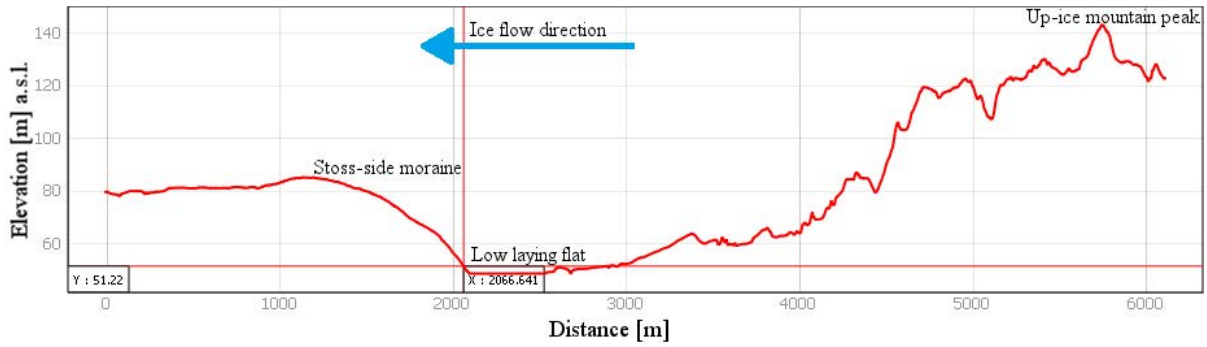

Figure C:10. Profile of the stoss-side moraine located at (N: 6352993 E: 353900).

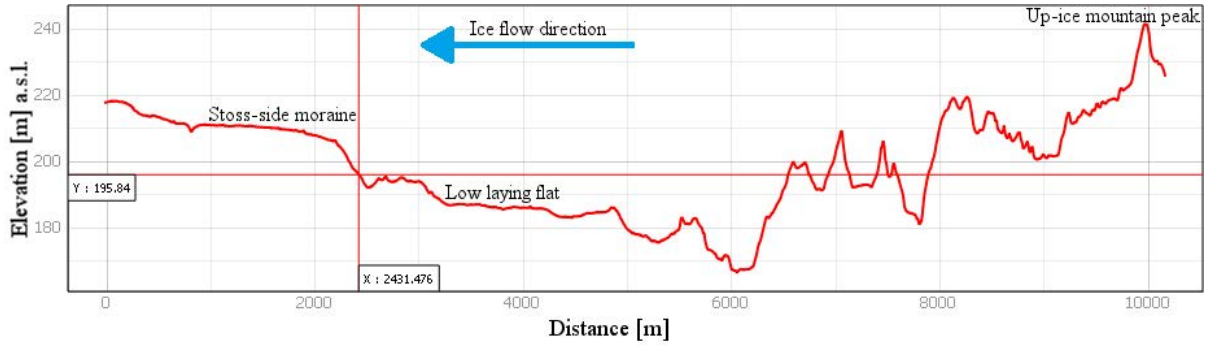

Figure C:11. Profile of the stoss-side moraine located at (N: 6391514 E: 392397).

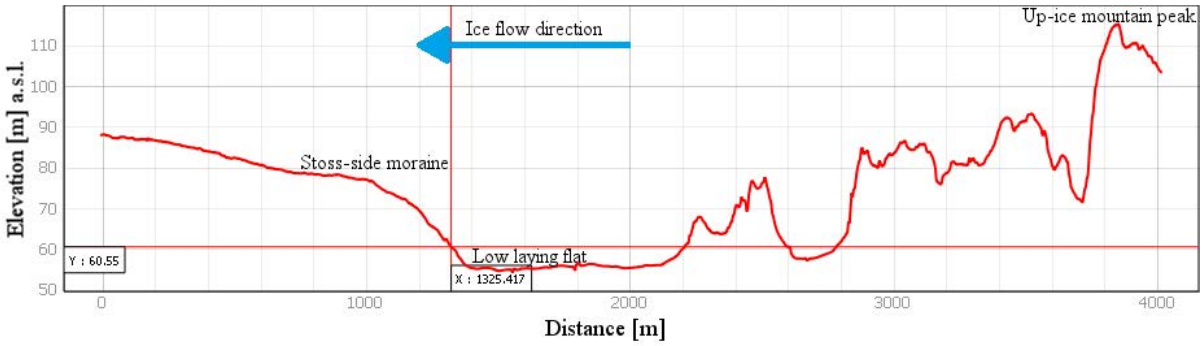

Figure C:12. Profile of the stoss-side moraine located at (N: 6366100 E: 336320).

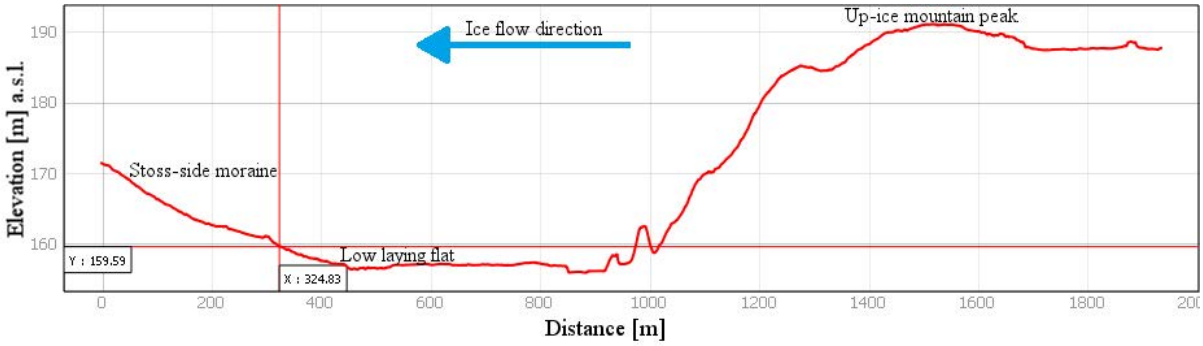

Figure C:13. Profile of the stoss-side moraine located at (N: 6385961 E: 388564).

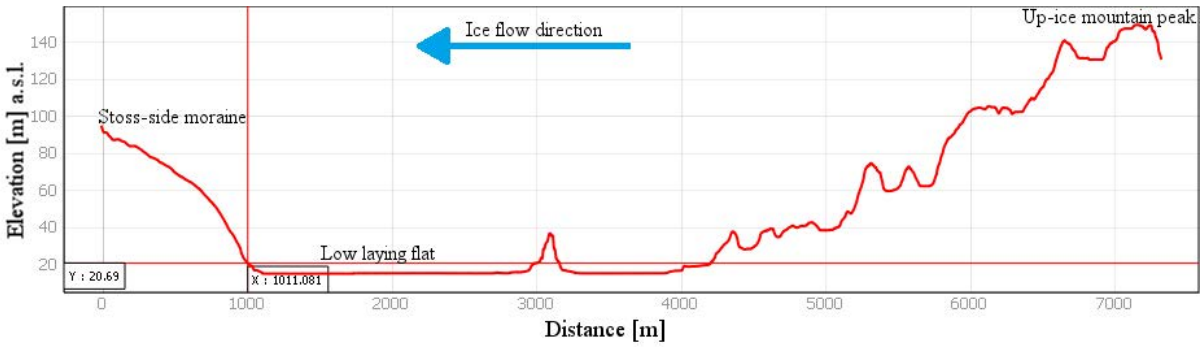

Figure C:14. Profile of the stoss-side moraine located at (N: 6352048 E: 349155).

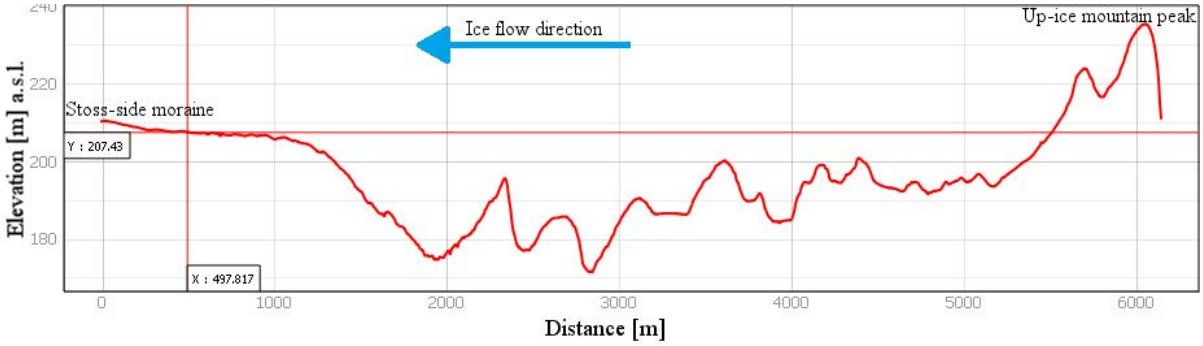

Figure C:15. Profile of the stoss-side moraine located at (N: 6368994 E: 381052).

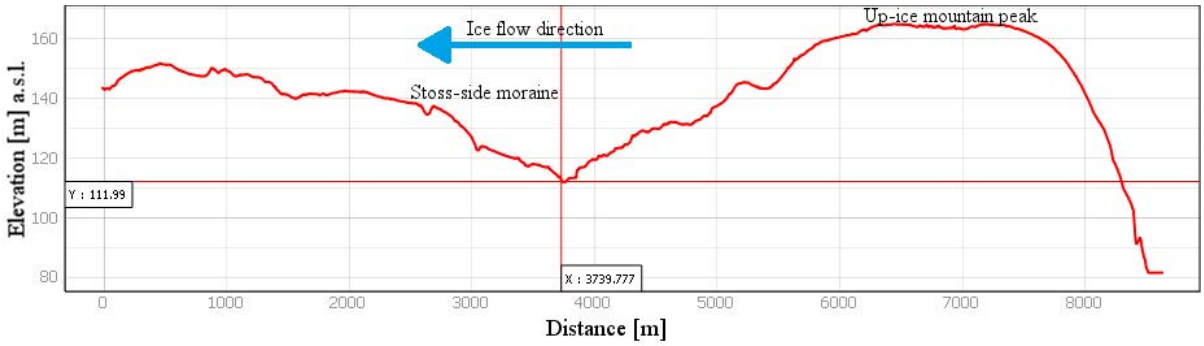

Figure C:16. Profile of the stoss-side moraine located at (N: 6384929 E: 341747).

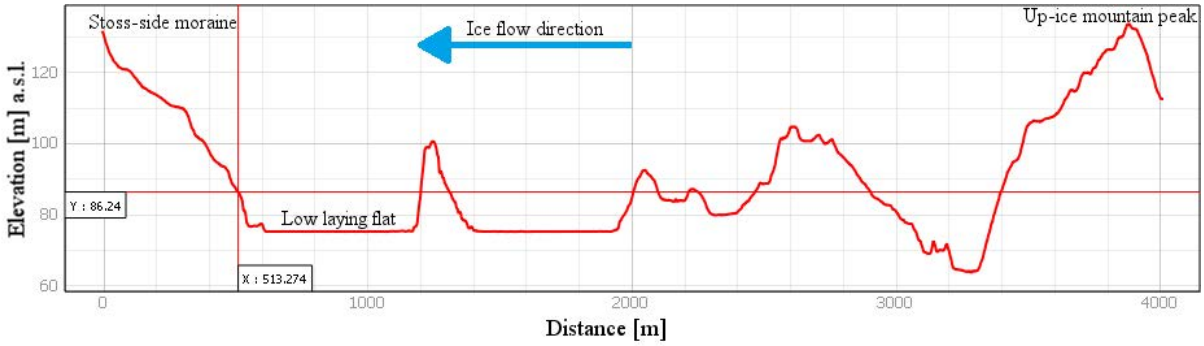

Figure C:17. Profile of the stoss-side moraine located at (N: 6329915 E: 353814).

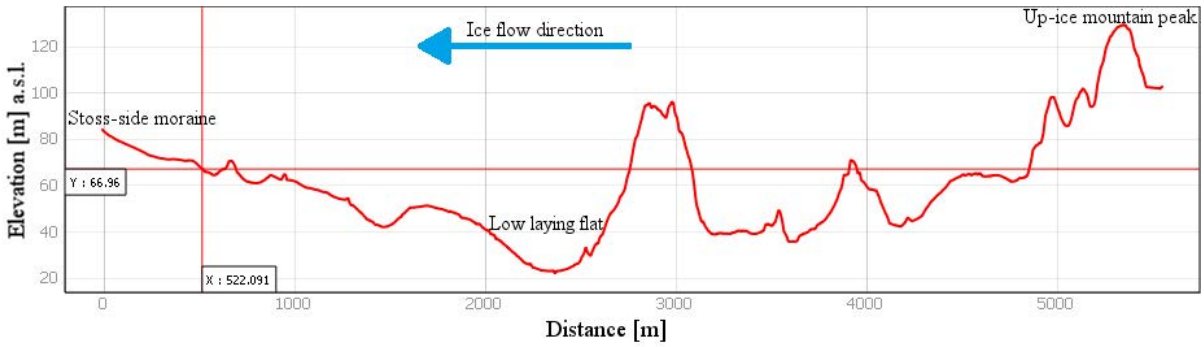

Figure C:18. Profile of the stoss-side moraine located at (N: 6340766 E: 344960).

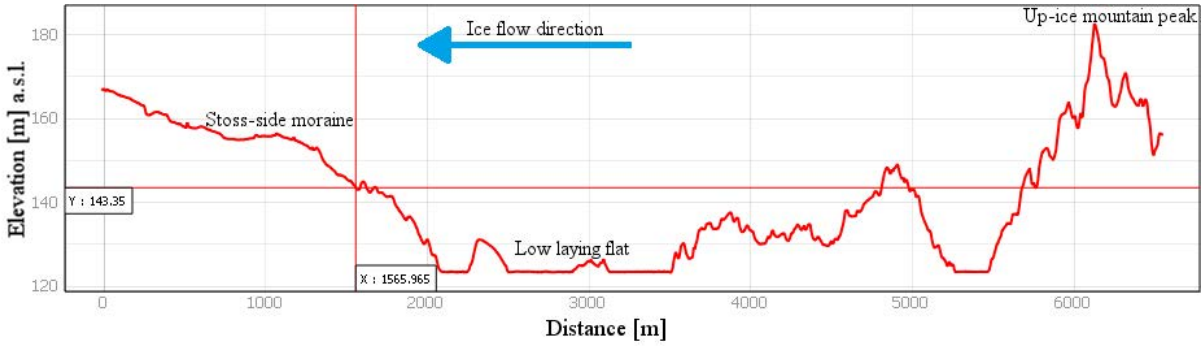

Figure C:19. Profile of the stoss-side moraine located at (N: 6407254 E: 349577).

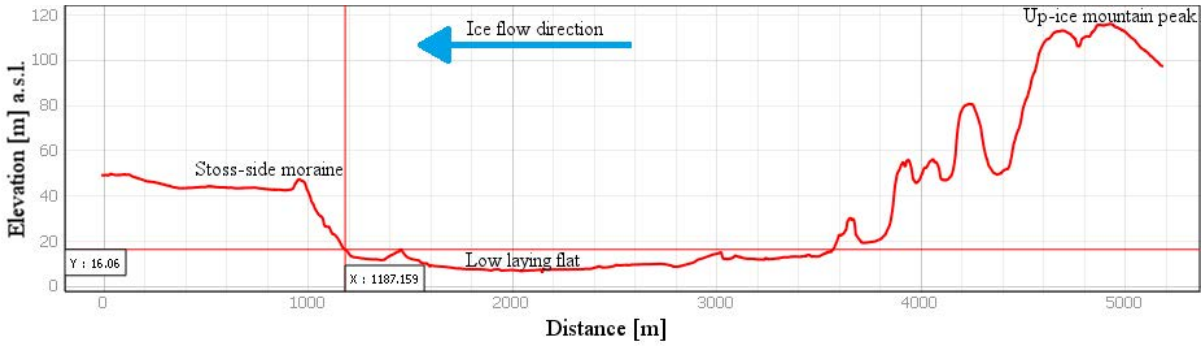

Figure C:20. Profile of the stoss-side moraine located at (N: 6341621 E: 336016).

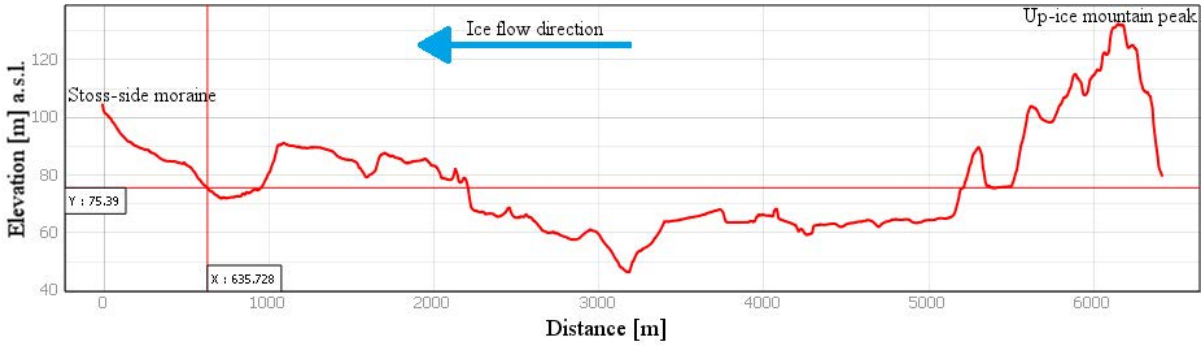

Figure C:21. Profile of the stoss-side moraine located at (N: 6328863 E: 354511).

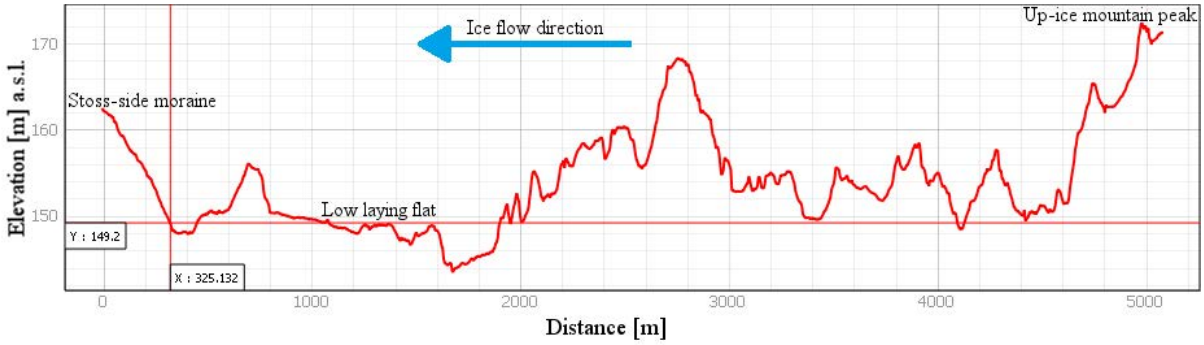

Figure C:22. Profile of the stoss-side moraine located at (N: 6390064 E: 376452).

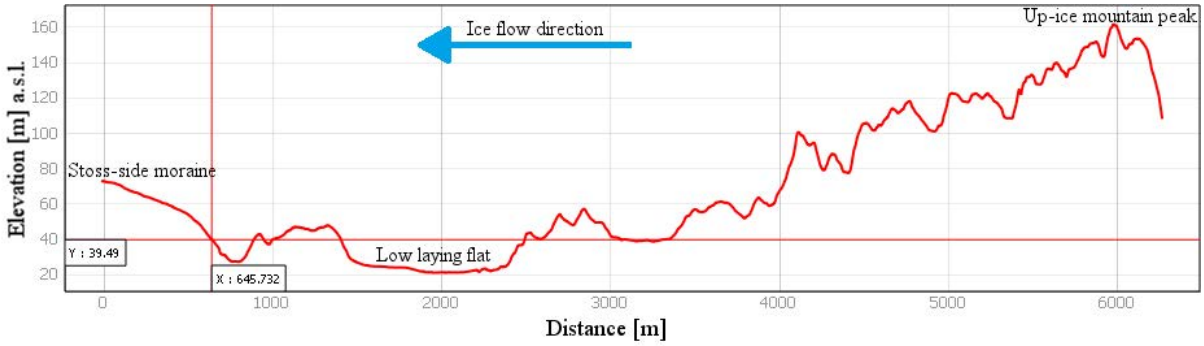

Figure C:23. Profile of the stoss-side moraine located at (N: 6341782 E: 345201).

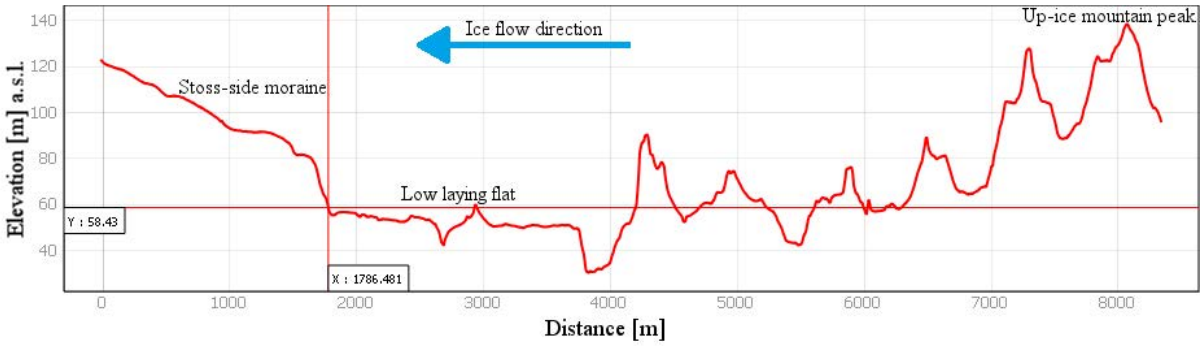

Figure C:24. Profile of the stoss-side moraine located at (N: 6327471 E: 354908).

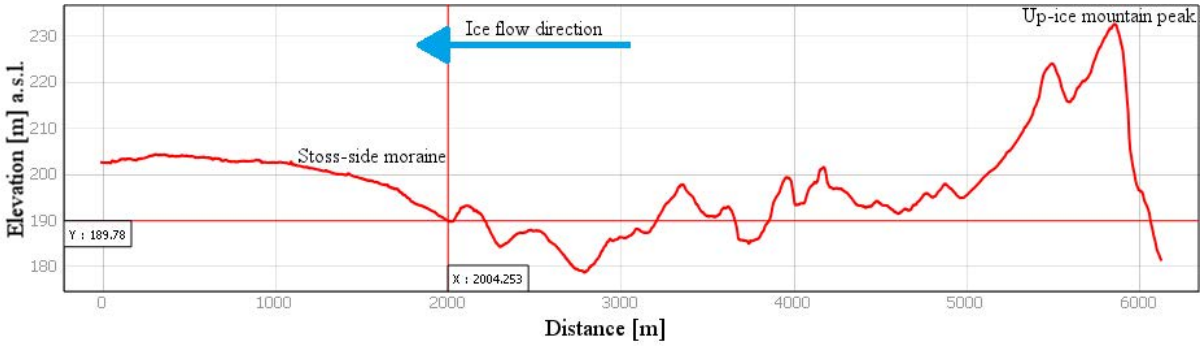

Figure C:25. Profile of the stoss-side moraine located at (N: 6369859 E: 381542).

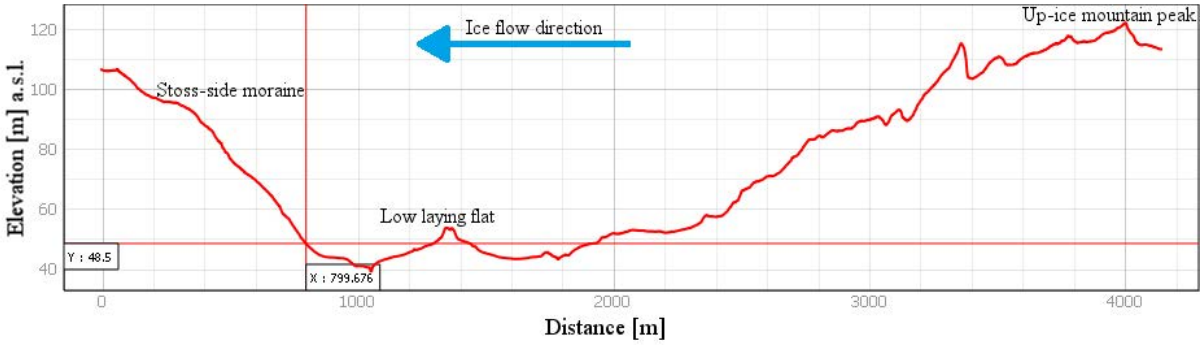

Figure C:26. Profile of the stoss-side moraine located at (N: 6371876 E: 346901).

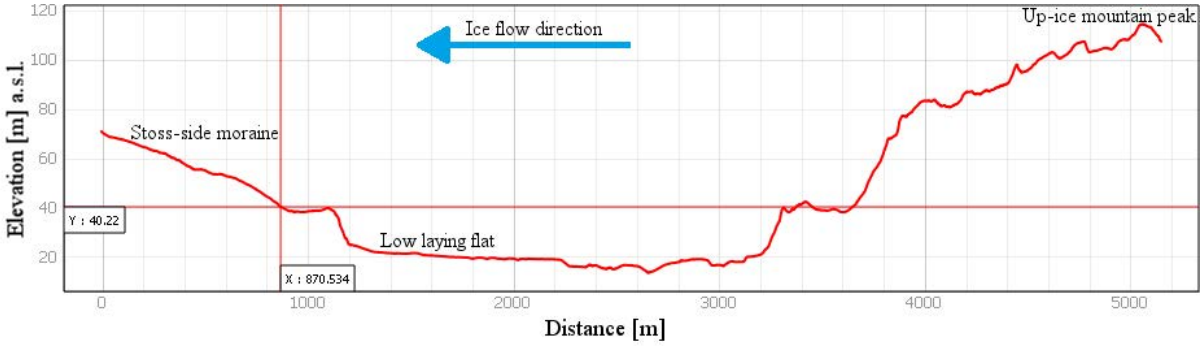

Figure C:27. Profile of the stoss-side moraine located at (N: 6355413 E: 349760).

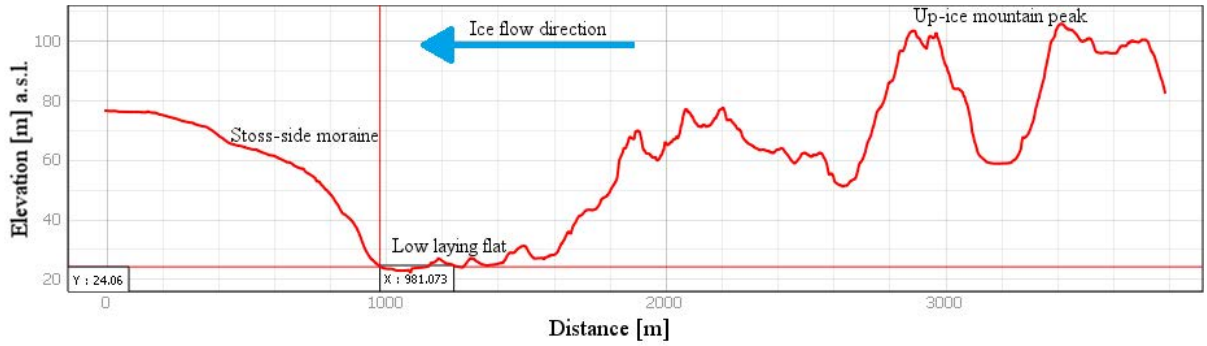

Figure C:28. Profile of the stoss-side moraine located at (N: 6341383 E: 346003).

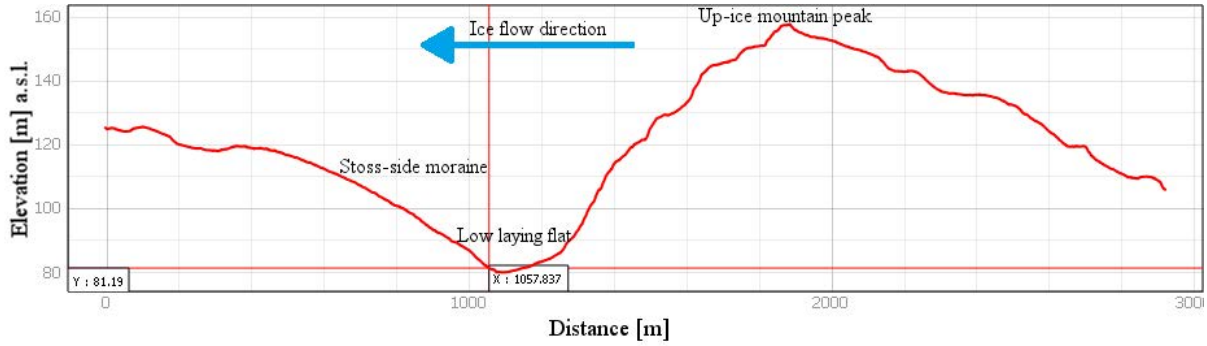

Figure C:29. Profile of the stoss-side moraine located at (N: 6331423 E: 351891).

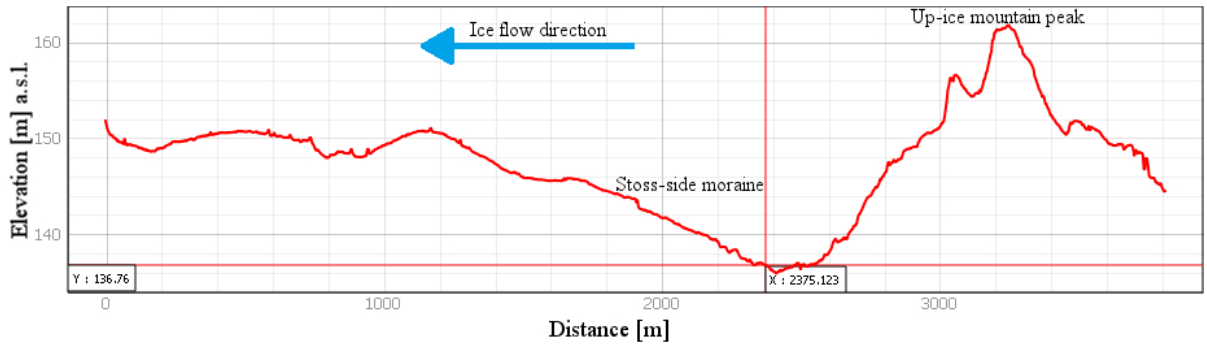

Figure C:30. Profile of the stoss-side moraine located at (N: 6383032 E: 339144).

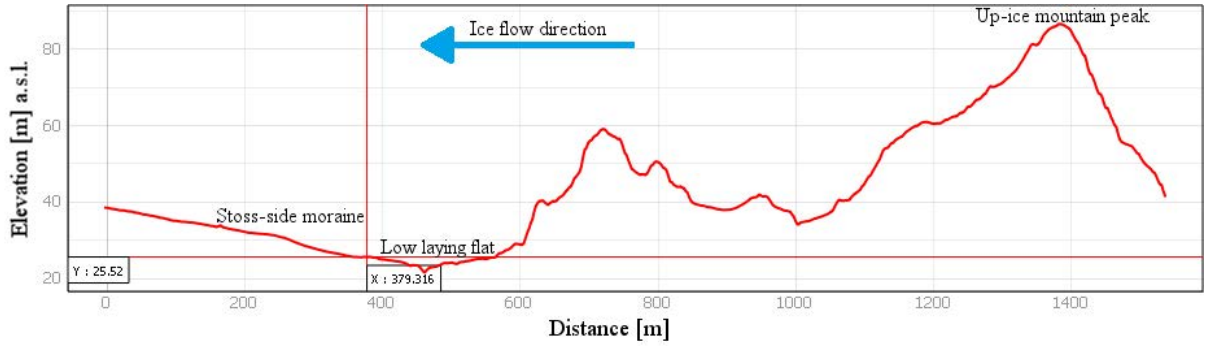

Figure C:31. Profile of the stoss-side moraine located at (N: 6342602 E: 346379).

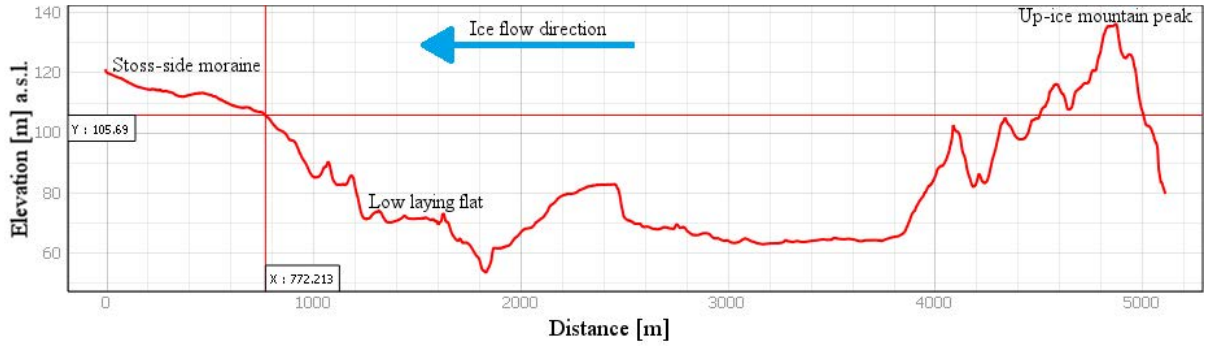

Figure C:32. Profile of the stoss-side moraine located at (N: 6330102 E: 355265).

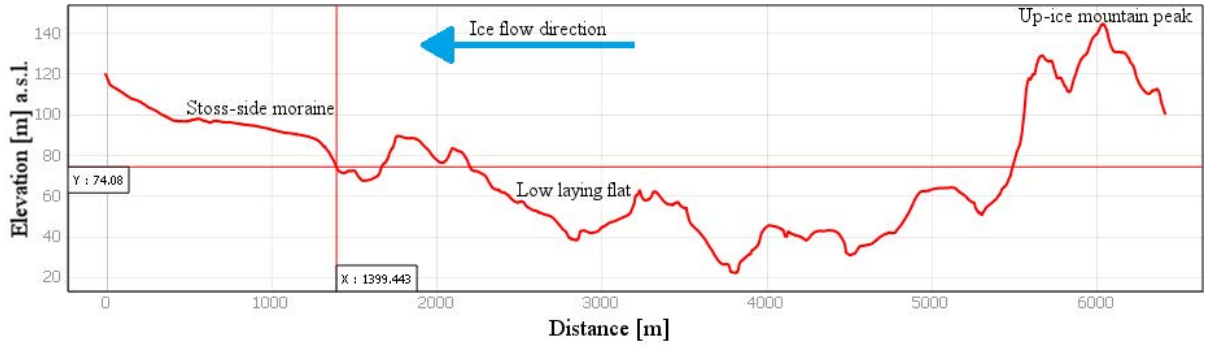

Figure C:33. Profile of the stoss-side moraine located at (N: 6325379 E: 355593).

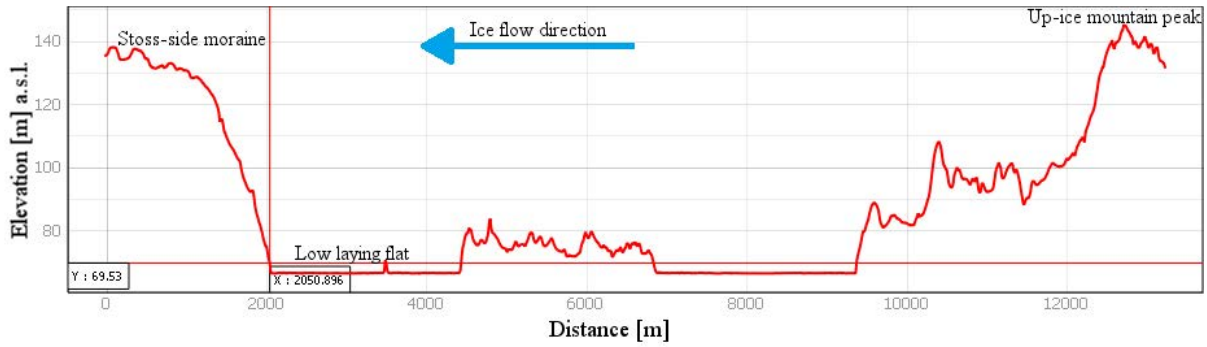

Figure C:34. Profile of the stoss-side moraine located at (N: 6434116 E: 349690).

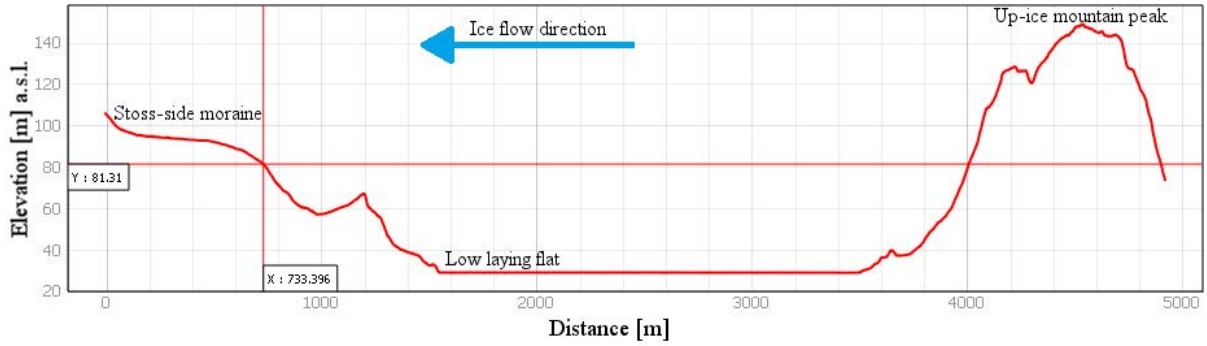

Figure C:35. Profile of the stoss-side moraine located at (N: 6357944 E: 339904).

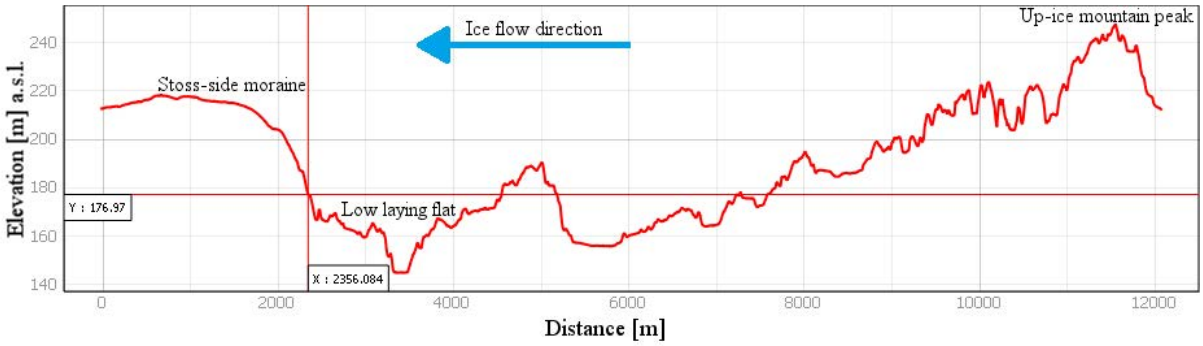

Figure C:36. Profile of the stoss-side moraine located at (N: 6410792 E: 354816).

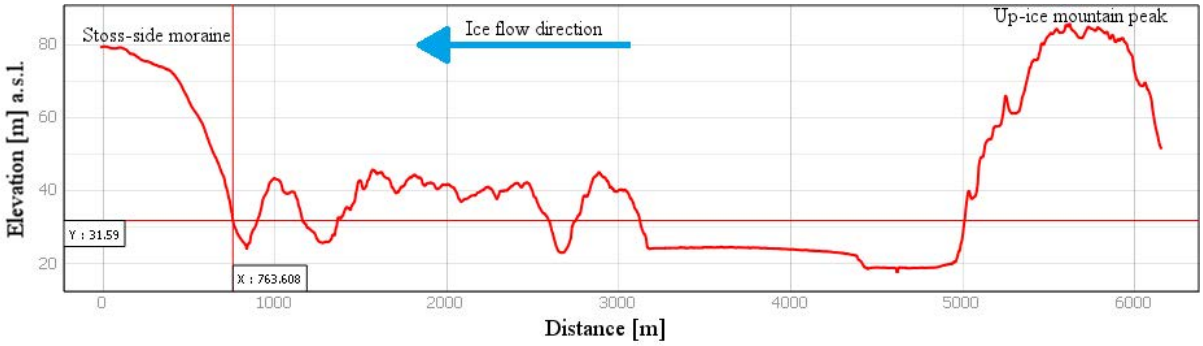

Figure C:37. Profile of the stoss-side moraine located at (N: 6340970 E: 341733).

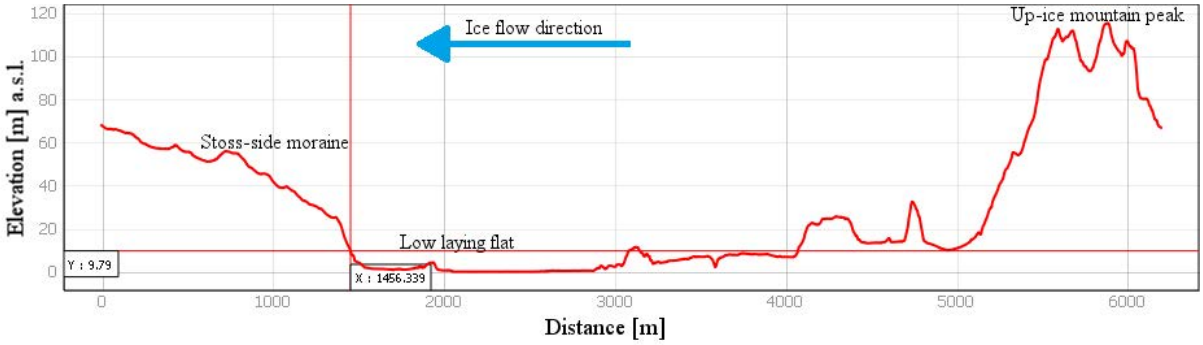

Figure C:38. Profile of the stoss-side moraine located at (N: 6418776 E: 322740).

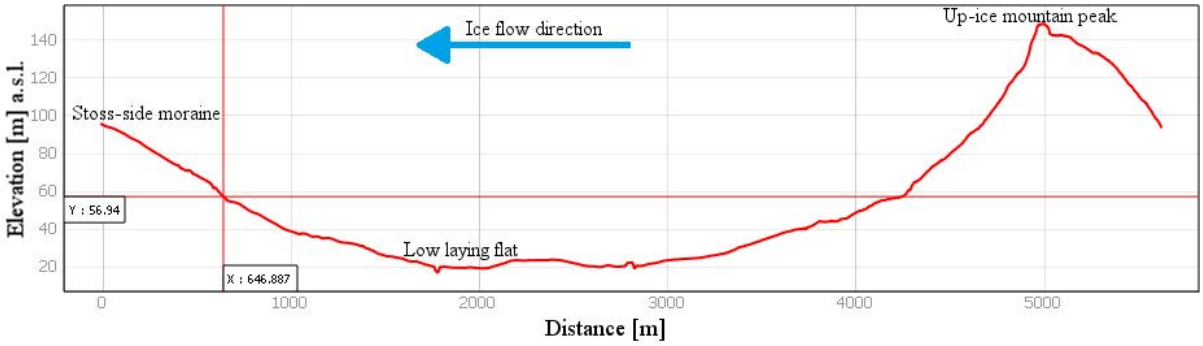

Figure C:39. Profile of the stoss-side moraine located at (N: 6294733 E: 363029).

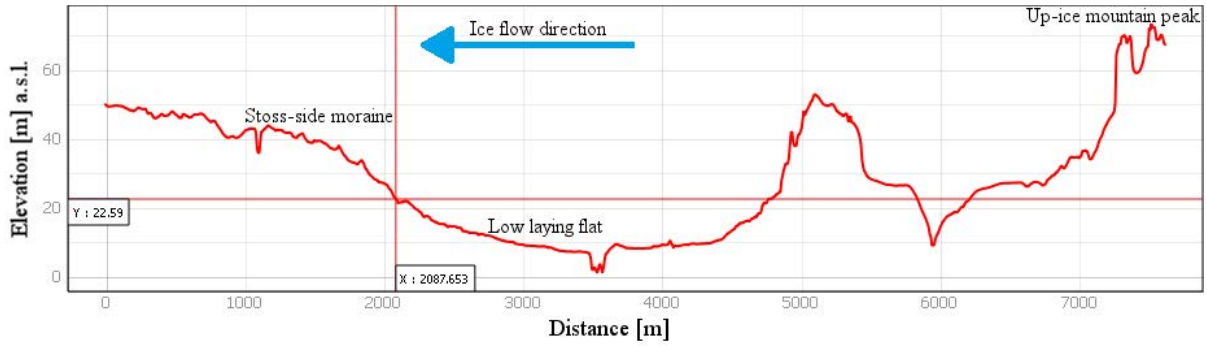

Figure C:40. Profile of the stoss-side moraine located at (N: 6428287 E: 331760).

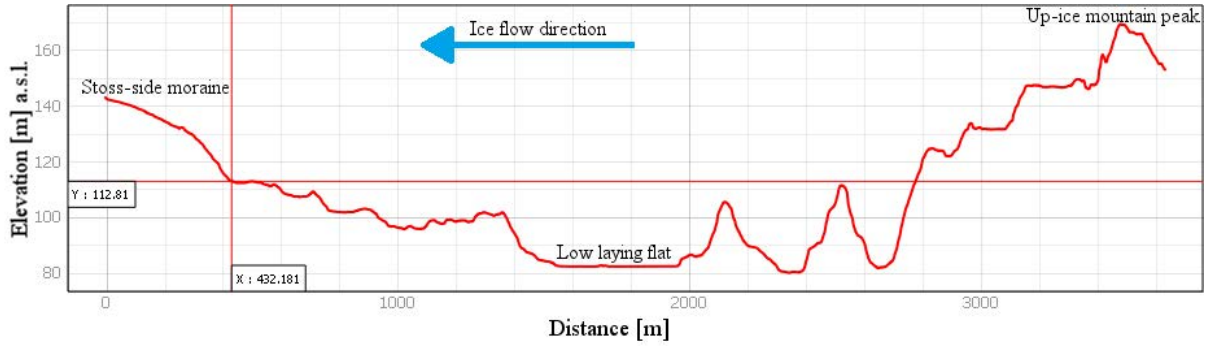

Figure C:41. Profile of the stoss-side moraine located at (N: 6381444 E: 355804).

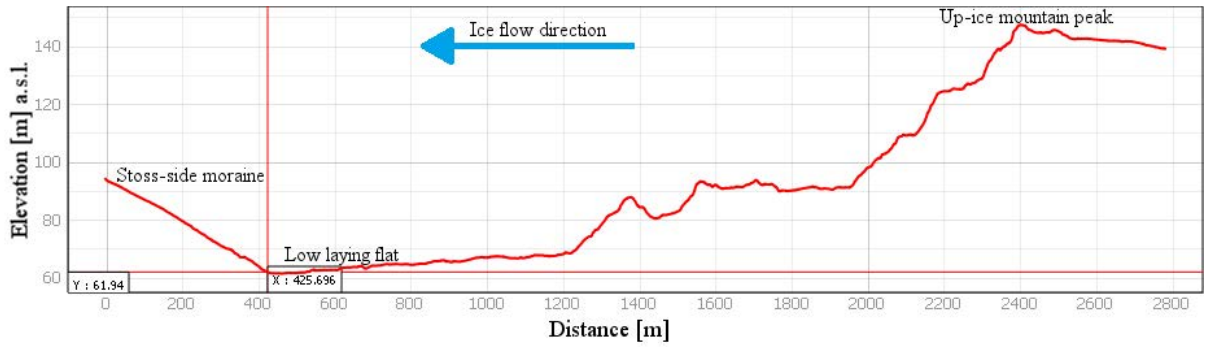

Figure C:42. Profile of the stoss-side moraine located at (N: 6311707 E: 361518).

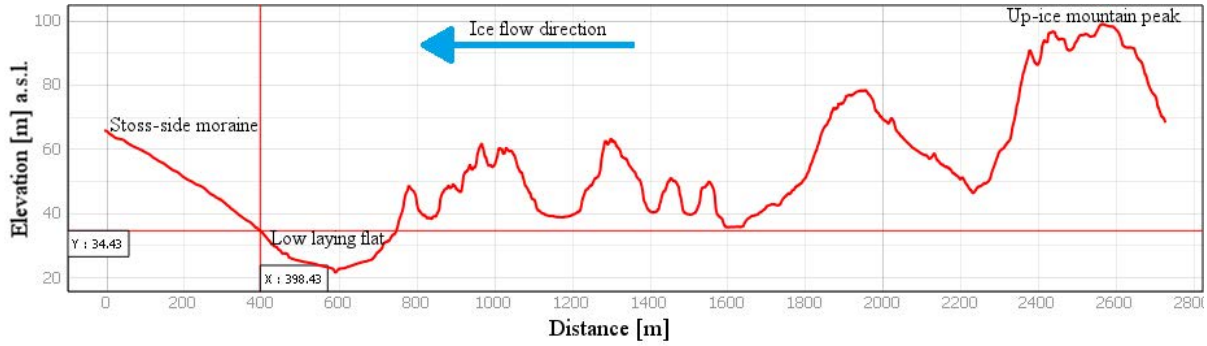

Figure C:43. Profile of the stoss-side moraine located at (N: 6342267 E: 346239).

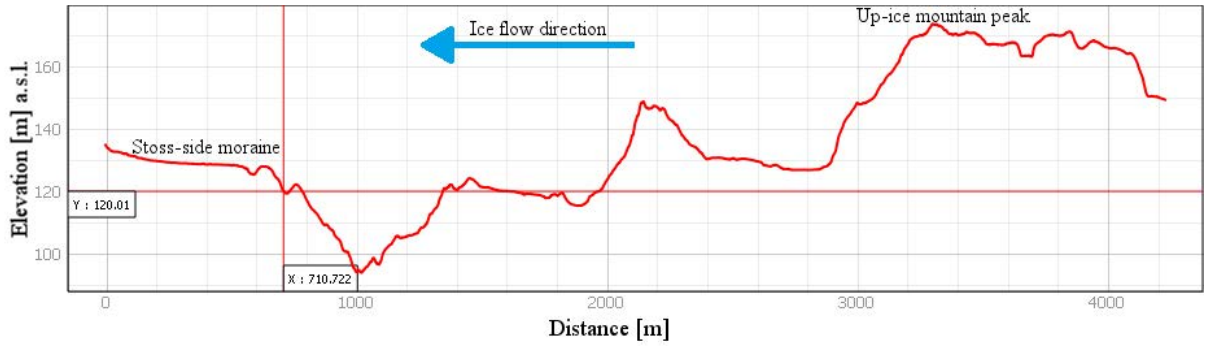

Figure C:44. Profile of the stoss-side moraine located at (N: 6310474 E: 362400).

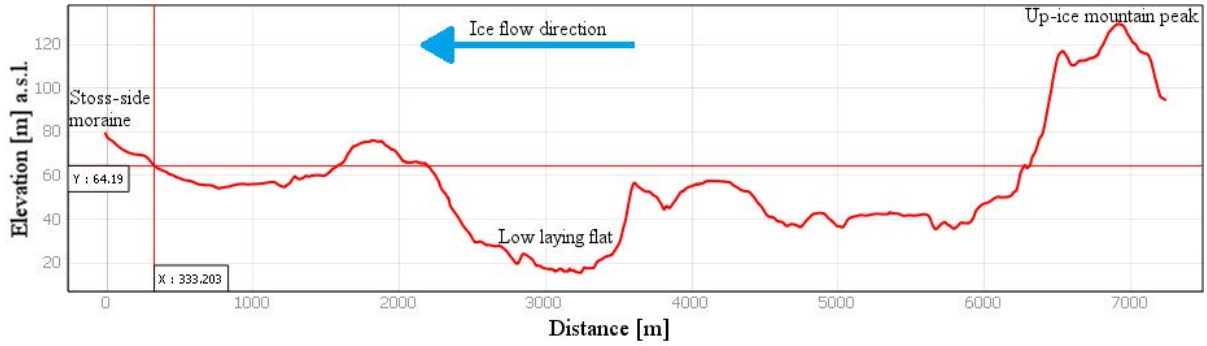

Figure C:45. Profile of the stoss-side moraine located at (N: 6318273 E: 354619).

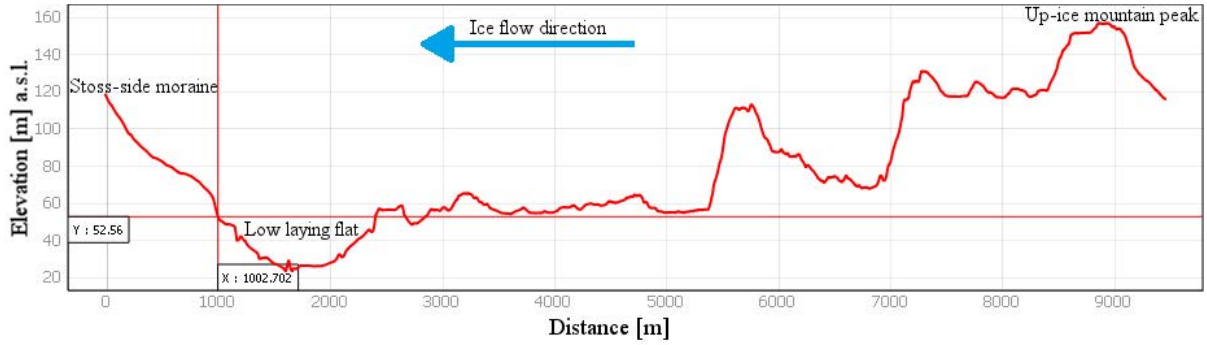

Figure C:46. Profile of the stoss-side moraine located at (N: 6292307 E: 367089).

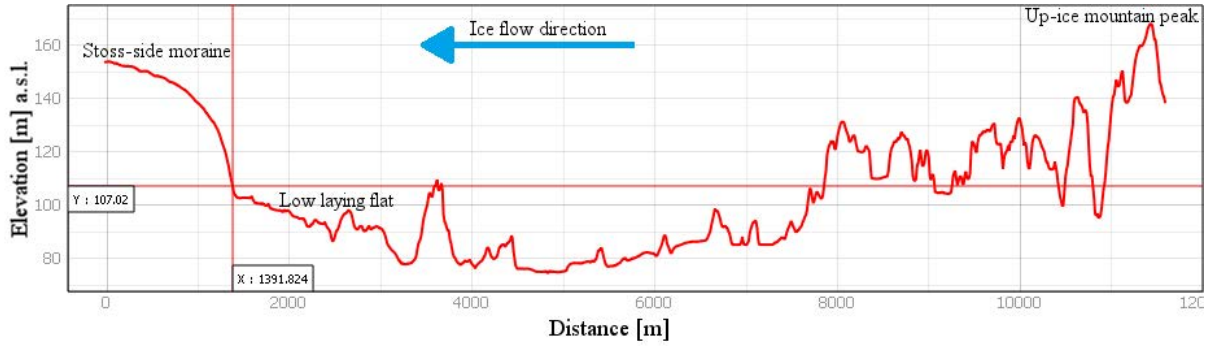

Figure C:47. Profile of the stoss-side moraine located at (N: 6377263 E: 357261).

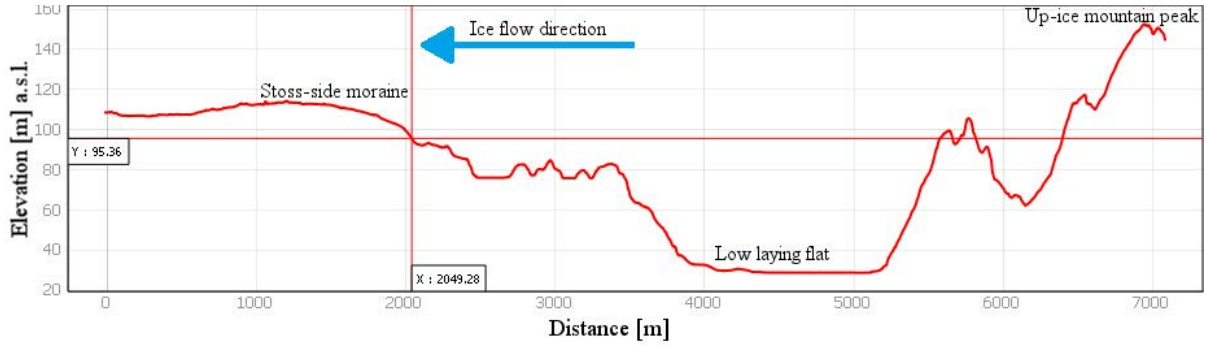

Figure C:48. Profile of the stoss-side moraine located at (N: 6358516 E: 344249).

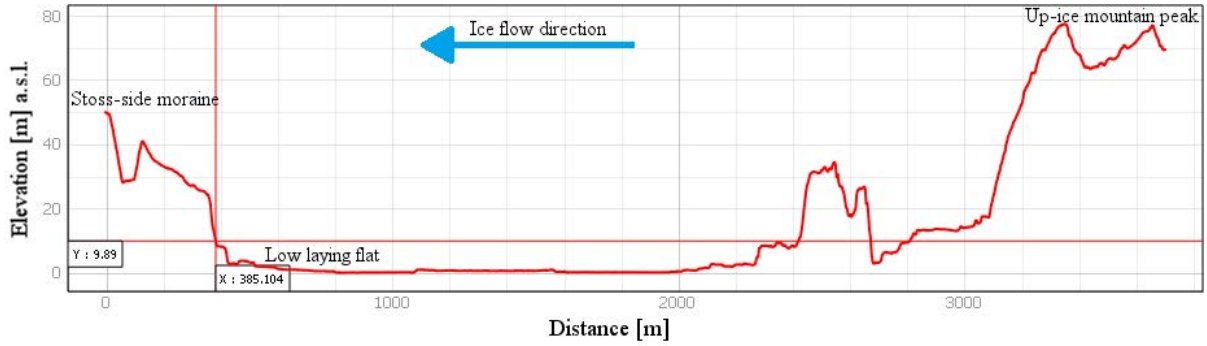

Figure C:49. Profile of the stoss-side moraine located at (N: 6416695 E: 321678).

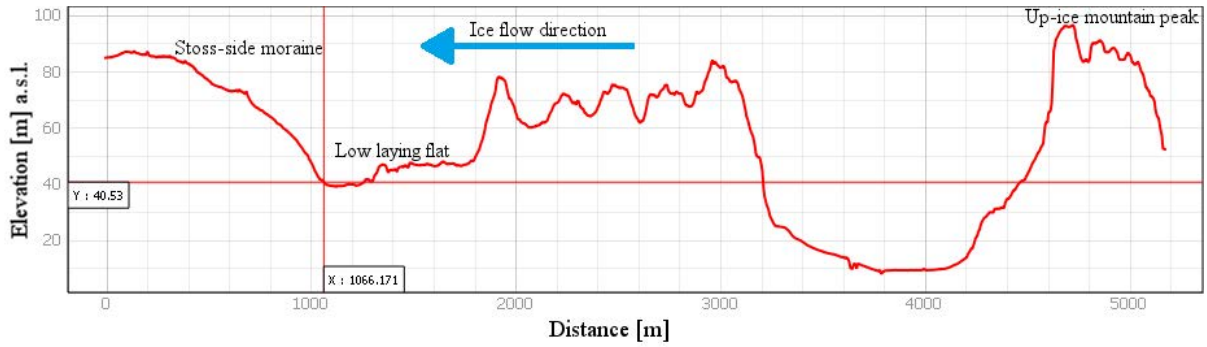

Figure C:50. Profile of the stoss-side moraine located at (N: 6381894 E: 322923).

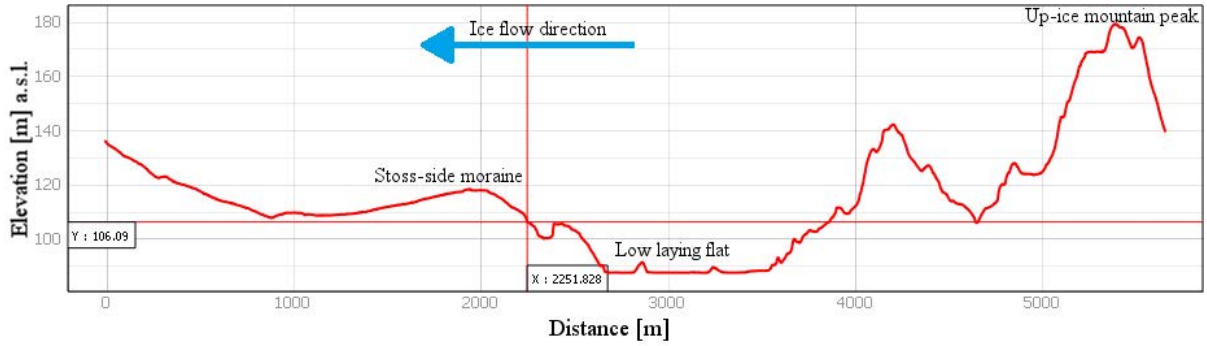

Figure C:51. Profile of the stoss-side moraine located at (N: 6333257 E: 351021).

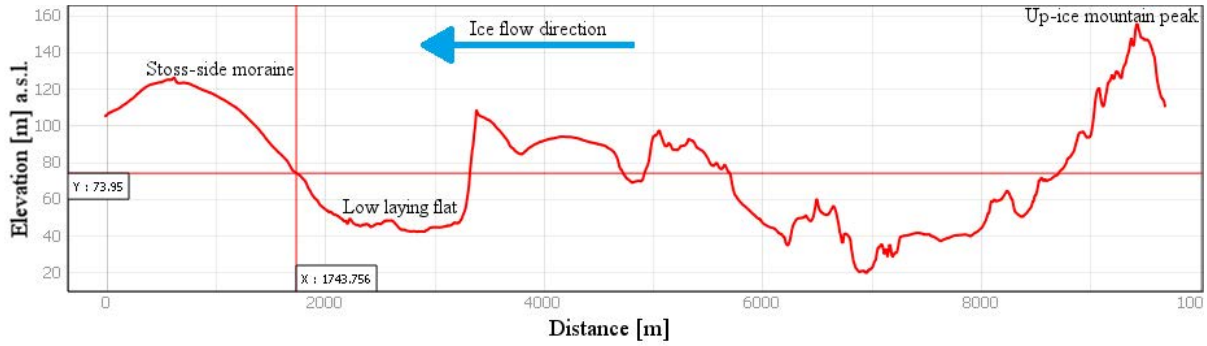

Figure C:52. Profile of the stoss-side moraine located at (N: 6323967 E: 352686).

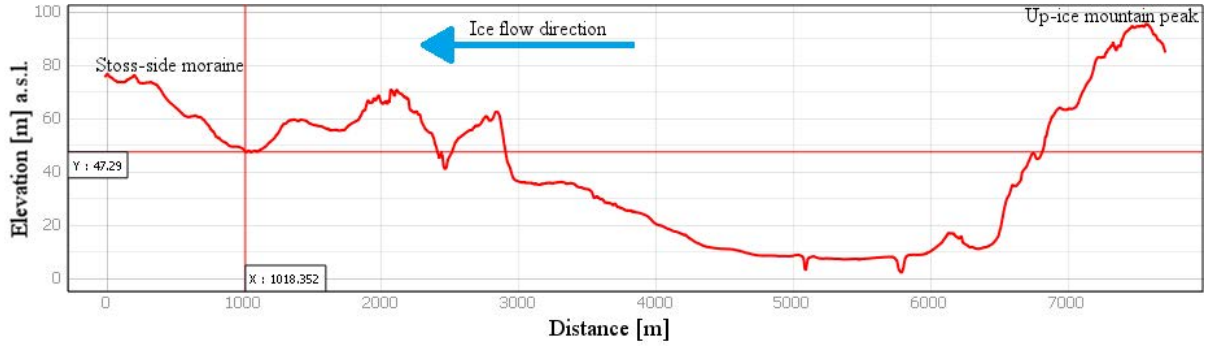

Figure C:53. Profile of the stoss-side moraine located at (N: 6423686 E: 322794).

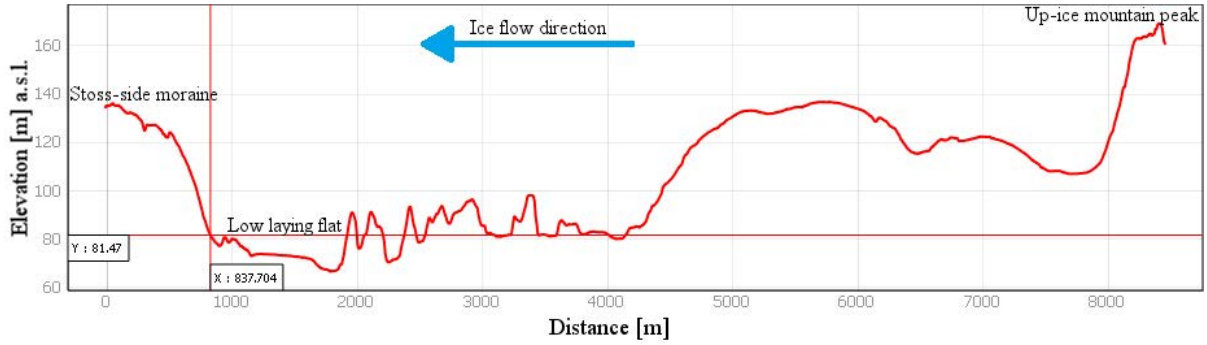

Figure C:54. Profile of the stoss-side moraine located at (N: 6365446 E: 341654).

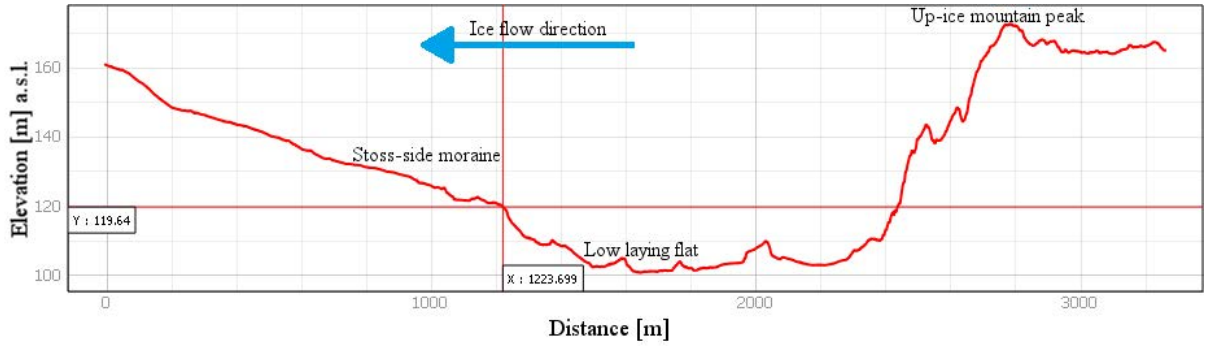

Figure C:55. Profile of the stoss-side moraine located at (N: 6427101 E: 365239).

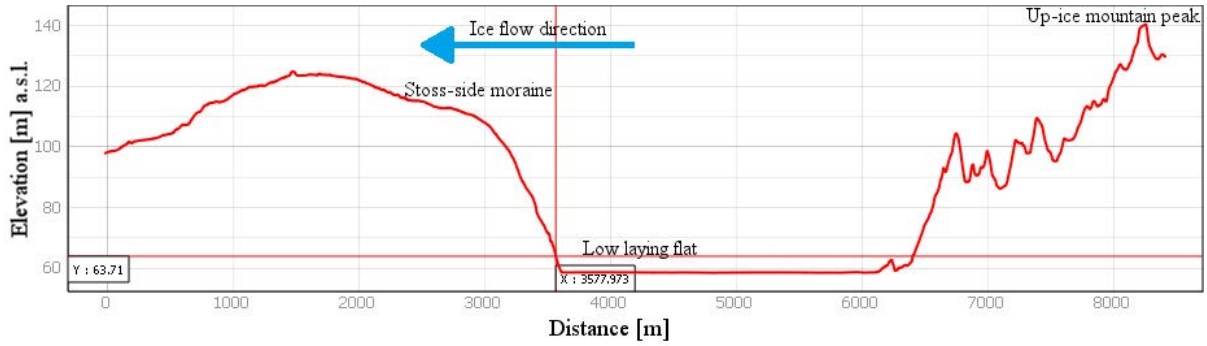

Figure C:56. Profile of the stoss-side moraine located at (N: 6369313 E: 358943).

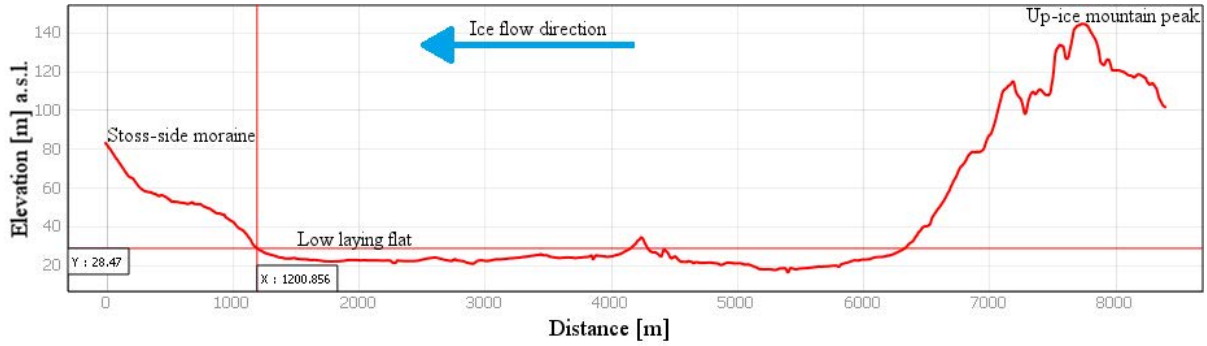

Figure C:57. Profile of the stoss-side moraine located at (N: 6296145 E: 358438).

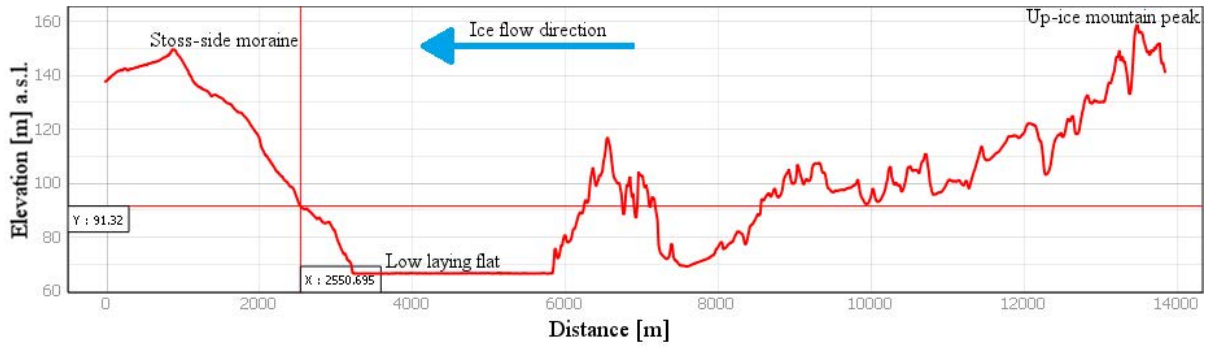

Figure C:58. Profile of the stoss-side moraine located at (N: 6436943 E: 349242).

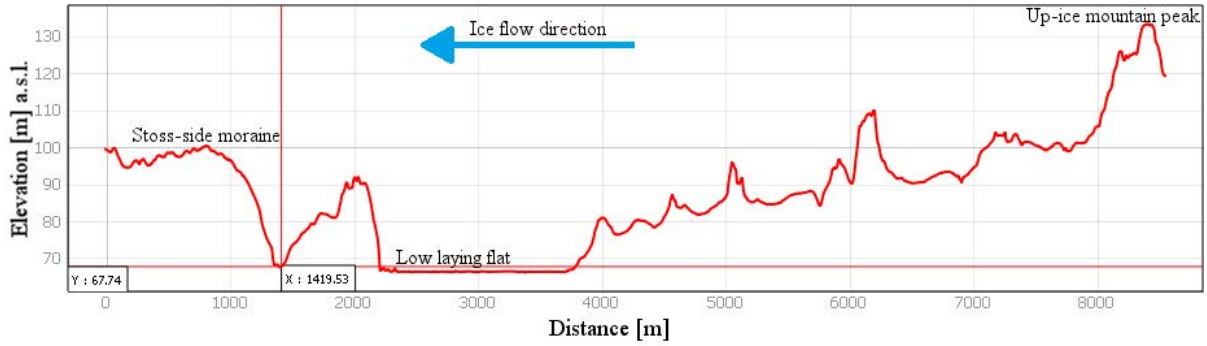

Figure C:59. Profile of the stoss-side moraine located at (N: 6437178 E: 354337).

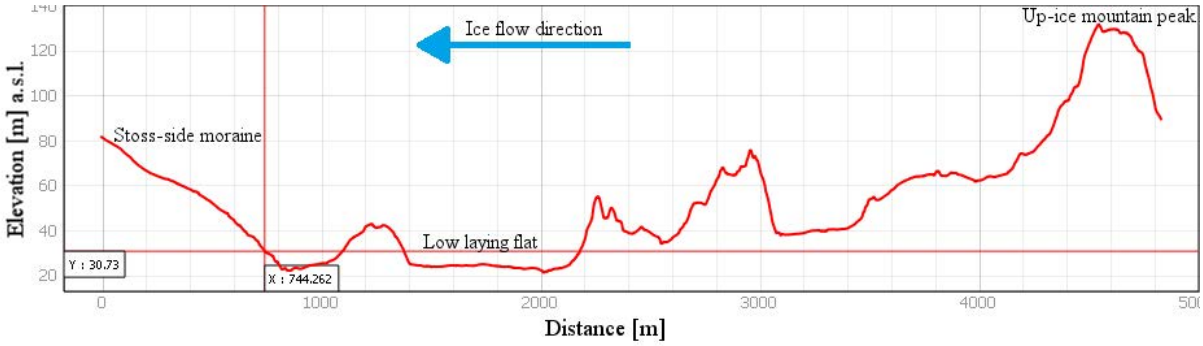

Figure C:60. Profile of the stoss-side moraine located at (N: 6342025 E: 345154).

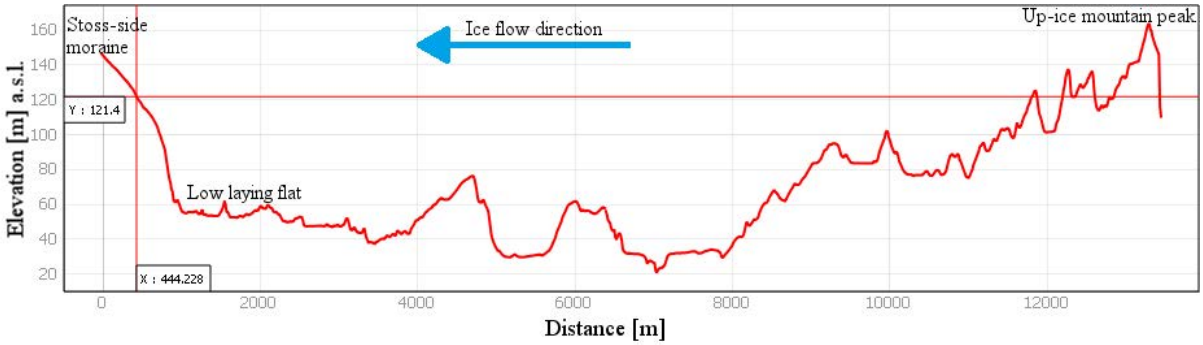

Figure C:61. Profile of the stoss-side moraine located at (N: 6368958 E: 344550).

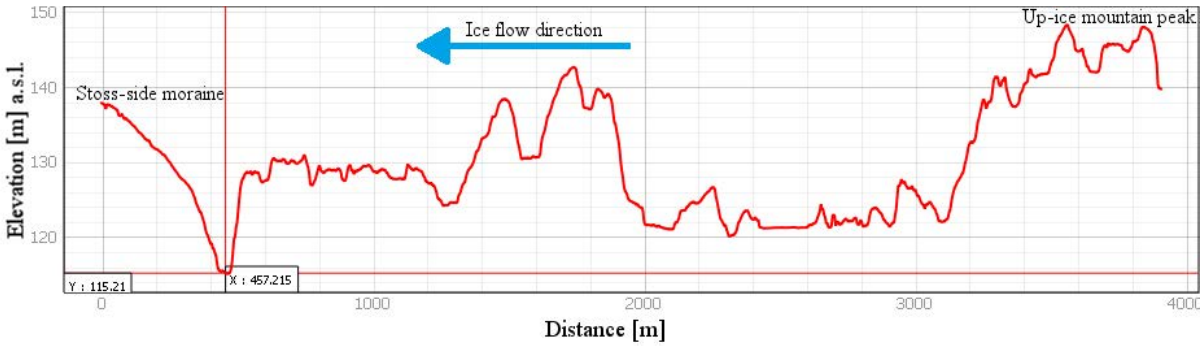

Figure C:62. Profile of the stoss-side moraine located at (N: 6414777 E: 330241).

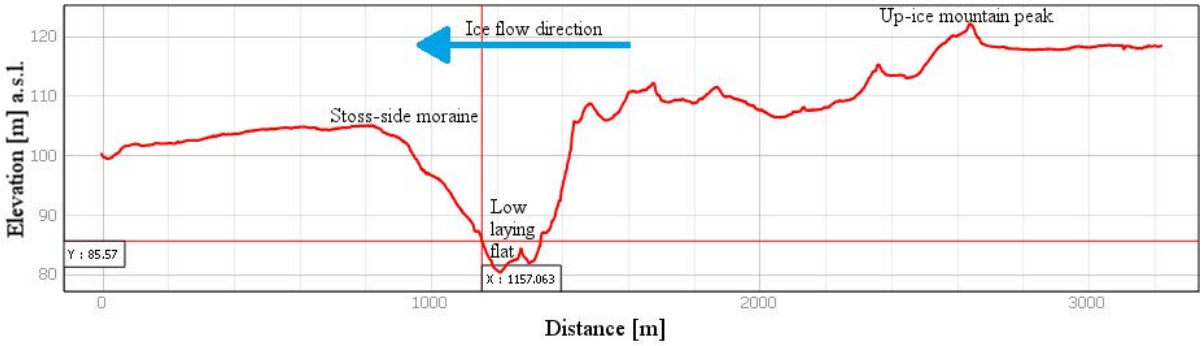

Figure C:63. Profile of the stoss-side moraine located at (N: 6368779 E: 356401).

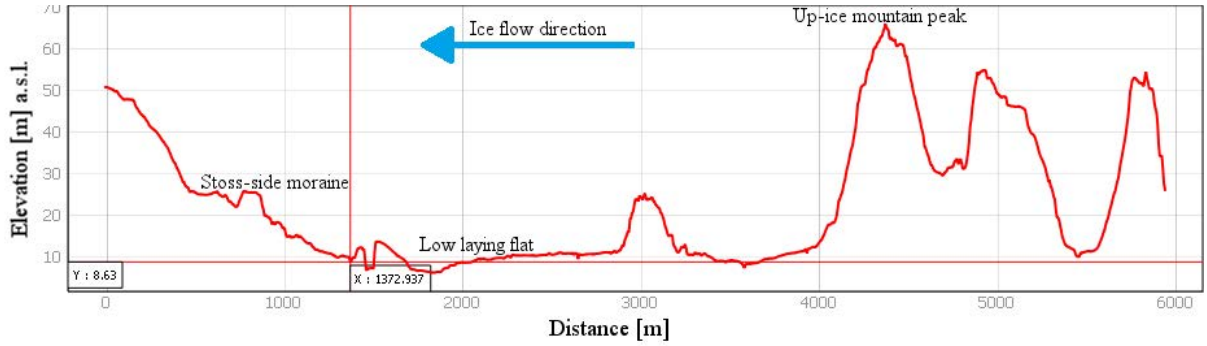

Figure C:64. Profile of the stoss-side moraine located at (N: 6418112 E: 319391).

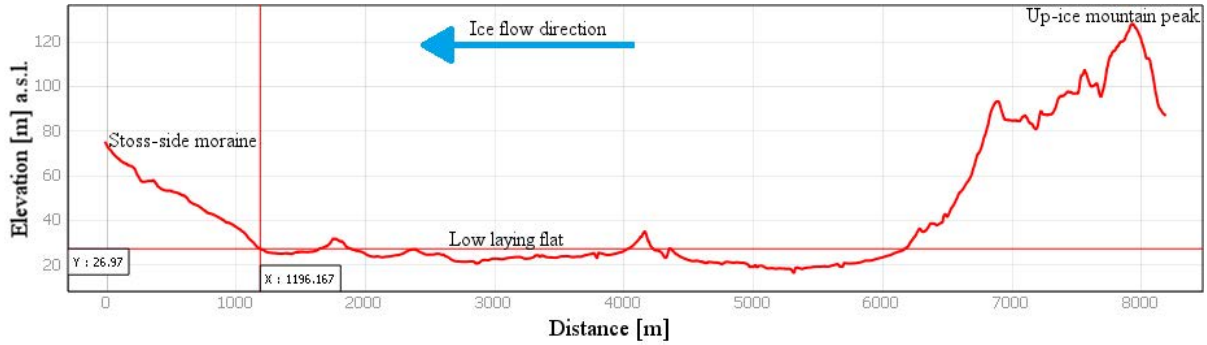

Figure C:65. Profile of the stoss-side moraine located at (N: 6296415 E: 358381).

Appendix D: The width of the bedrock knob of the landforms.

Width stoss-side moraines [m]	Width crag-and-tails [m]
77,10	16,60
127,10	16,6
148,90	16,70
157,90	16,7
178,90	21,70
184,10	21,7
190,40	21,90
192,70	21,9
193,50	22,40
204,20	23,50
213,80	24,50
216,40	27,20
225,70	28,10
233,10	28,40
248,20	28,70
249,20	29,30
262,80	30,20
266,90	30,50
268,20	30,90
268,80	32,40
284,80	34,20
318,50	34,40
319,50	35,30
331,50	39,10
331,70	42,30
337,80	43,10
343,90	43,70
344,60	44
348,30	45,70
353,80	47,40
374,90	49
401,50	51,10
411,60	52,10
428,20	53,30
448,10	54,10
459,40	54,80

467,40	55,10
499	57,60
509,90	59,20
514,20	59,50
521,10	59,90
564,70	60,40
566,10	61,30
577,50	61,70
606,90	62,40
651,90	70,70
672,70	71,60
676,90	71,70
677,40	72,40
679,40	75,30
679,90	75,60
684,80	77
693,70	86,80
710,20	88,10
731,40	88,80
748,20	90,50
752	91,80
779,70	113,10
783,60	115,10
814,10	127,50
821,30	
824,10	
841,70	
842,70	
843,60	
856,80	
871,90	
883,80	
959,70	
1012	
1123	
1 497,60	
1 517,20	

Table D:1. The width of the grounding bedrock knob that the landforms form around. Sorted from most narrow to widest. All units are in meters.